

Densest binary sphere packings

Adam B. Hopkins and Frank H. Stillinger

Department of Chemistry, Princeton University, Princeton, New Jersey 08544, USA

Salvatore Torquato

Department of Chemistry, Department of Physics, Princeton Center for Theoretical Science, Princeton Institute for the Science and Technology of Materials, Program in Applied and Computational Mathematics, Princeton University, Princeton, New Jersey 08544, USA

(Received 17 November 2011; published 22 February 2012)

The densest binary sphere packings in the α - x plane of small to large sphere radius ratio α and small sphere relative concentration x have historically been very difficult to determine. Previous research had led to the prediction that these packings were composed of a few known “alloy” phases including, for example, the AIB₂ (hexagonal ω), HgBr₂, and AuTe₂ structures, and to XY_{*n*} structures composed of close-packed large spheres with small spheres (in a number ratio of n to 1) in the interstices, *e.g.*, the NaCl packing for $n = 1$. However, utilizing an implementation of the Torquato-Jiao sphere-packing algorithm [Torquato and Jiao, *Phys. Rev. E* **82**, 061302 (2010)], we have discovered that many more structures appear in the densest packings. For example, while all previously known densest structures were composed of spheres in small to large number ratios of one to one, two to one, and very recently three to one, we have identified densest structures with number ratios of seven to three and five to two. In a recent work [Hopkins *et al.*, *Phys. Rev. Lett.* **107**, 125501 (2011)], we summarized these findings. In this work, we present the structures of the densest-known packings and provide details about their characteristics. Our findings demonstrate that a broad array of different densest mechanically stable structures consisting of only two types of components can form without any consideration of attractive or anisotropic interactions. In addition, the structures that we have identified may correspond to currently unidentified stable phases of certain binary atomic and molecular systems, particularly at high temperatures and pressures.

DOI: [10.1103/PhysRevE.85.021130](https://doi.org/10.1103/PhysRevE.85.021130)

PACS number(s): 64.10.+h, 61.50.-f, 61.66.Dk, 81.30.Fb

I. INTRODUCTION

A packing is defined as a set of nonoverlapping objects arranged in a space of given dimension d , and its packing fraction ϕ is the fraction of space that the objects cover. Packings of spheres in d -dimensional Euclidean space \mathbb{R}^d are frequently used as starting points in modeling atomic, molecular, and granular materials consisting of particles exhibiting strong repulsive pair interactions at small particle separations. In particular, the densest sphere packings in \mathbb{R}^d , or packings with maximal packing fraction ϕ_{\max} , often correspond to ground states of systems of particles with pairwise interactions dominated by steep isotropic pairwise repulsion [1]. For example, see the ground states in Refs. [2–7].

Packings of identical spheres have been employed in \mathbb{R}^3 to describe the structures and some fundamental properties of a diverse range of substances from crystals and colloids to liquids, amorphous solids, and glasses [8–11]. Despite their simplicity, complicated structures and interesting properties can arise in packings of identical spheres through simple principles like density maximization in a confined space [12,13]. Packings of identical nonspherical objects in \mathbb{R}^3 have also been studied, though not to the extent of sphere packings, and have applications, for example, in the self-assembly of colloids and nanoparticles [14–20]. In structural biology, molecular dynamics simulations of interactions between large numbers of molecules employ chains of identical nonoverlapping spheres as models for various biological structures such as proteins and lipids [21], and packing of nonspherical objects of different sizes are used, for example, in tumor growth modeling [22,23].

Packings of spheres of many different sizes have been employed as structural models for materials such as solid

propellants and concrete, among others [24,25]. Dense binary packings of spheres, packings of spheres of only two sizes, have long been employed as models for the structures of a wide range of alloys [3,26–32]. In this work, we focus on binary sphere packings. Though they are relatively simple models, much about them is still unknown due in part to the enormous binary sphere-packing parameter space of sphere size ratio and relative concentration. Recently, we presented a comprehensive determination of the “phase diagram” in small to large sphere size ratio α and small sphere relative concentration x for the densest binary sphere packings in \mathbb{R}^3 [33]. In the present paper, we extend these results to produce an updated phase diagram, and we present a theorem and proof concerning the number of phases present in a densest packing with η different types of objects. Additionally, we present detailed structural descriptions of the alloy phases present in the densest packings, identified using the Torquato-Jiao (TJ) determinantal sphere-packing algorithm [34], including descriptions of many that were heretofore unknown. Here we use the term “alloy” in a general sense to mean a structure composed of two or more distinguishable components that are not phase separated.

Structures, or configurations of points, can be classified as either periodic or aperiodic. Roughly defined, a *periodic* structure (packing) is one consisting of a certain number of points (sphere centers), called the *basis*, placed in a defined region of space, the *unit cell*, replicated many times over such that the cells cover all space without any overlap between cells (or spheres). A *fundamental cell* is one with *minimal basis*, *i.e.*, such that a smaller fundamental cell and basis with the same periodic structure does not exist. An *aperiodic* structure is one with an infinite (or in practice, very large finite) minimal

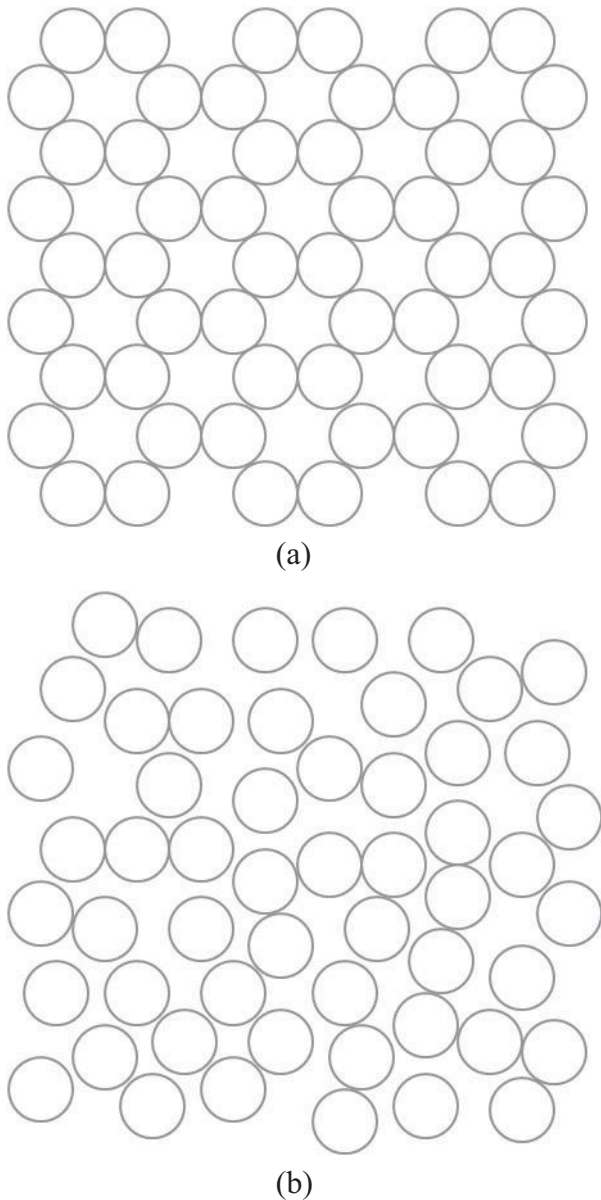


FIG. 1. Illustrations of subsections of packings of disks that are (a) periodic and (b) aperiodic.

basis. By definition, it is clear that a binary sphere packing must have at least two spheres in its minimal basis. Figure 1 is an illustration that compares subsections of periodic and aperiodic packings of monodisperse disks.

The packing fraction $\phi_{\max}(\alpha, x)$ of the densest binary packings of spheres in \mathbb{R}^3 is a function only of small to large sphere radius ratio $\alpha = R_S/R_L$, with R_S and R_L the respective radii of the small and large spheres, and small sphere relative concentration x . Specifically, one has

$$x \equiv \frac{N_S}{N_S + N_L}, \quad (1)$$

with N_S and N_L the respective numbers of small and large spheres in the packing, and when $N_S + N_L \rightarrow \infty$ in the infinite volume limit, x remains constant. It is implicit in the definition of $\phi_{\max}(\alpha, x)$ that radii are additive, *i.e.*, two spheres of different radii can be no closer than distance $R_S + R_L$ from

one another. In this work, we focus on the additive case, though we note that the TJ algorithm can be trivially modified to study sphere packings with nonadditive diameters. Past studies of certain sphere packings with nonadditive diameters can be found, for example, in Ref. [35].

The densest packings in \mathbb{R}^3 are composed of a countable number of distinct phase-separated alloy and monodisperse phases. Previously, the only alloys thought to be present in the densest packings for $\alpha > \sqrt{2} - 1 = 0.414213\dots$ corresponded to structures such as the A_3B , AlB_2 (hexagonal ω), $HgBr_2$, and $AuTe_2$ structures [27,36–38], and to a structure composed of equal numbers of small and large spheres [39]. For $\alpha \leq \sqrt{2} - 1$, the alloys thought to be present were XY_n structures of close-packed large spheres with small spheres (in a ratio of n to 1) in the interstices, *e.g.*, the NaCl packing for $n = 1$. However, in a recent work [33], we showed that in addition to these alloys, many more are present in the putative densest packings, including several with heretofore unknown structures.

The densest binary packings of spheres can be directly relevant to atomic and molecular phases in binary solids and compounds. For example, structures such as that exhibited by AlB_2 have been predicted and observed to be present in high temperature and pressure phases of various binary intermetallic and rare-gas compounds [40,41]. Furthermore, phase separation of alloys like that present in the densest binary packings has been observed in certain binary atomic and molecular solids at high temperatures and pressures, conditions where relaxation time scales are fast and diffusion rates high [42]. These observations indicate that the hard-sphere additive-radii interactions that lead to the densest binary sphere packings may be sufficient to determine the stable phases of many binary atomic and molecular solids and compounds at high temperatures and pressures. In addition, we believe that there are binary atomic and molecular systems, particularly at high temperatures and pressures, that will exhibit stable phases with structures corresponding to the heretofore unknown alloys described in Sec. V.

In the past, finding the densest packings has been difficult in part due to the complexity of proving that a packing of spheres in \mathbb{R}^d is the densest possible, evident in that Kepler's conjecture concerning the densest packings of monodisperse spheres in \mathbb{R}^3 was only recently proved by Hales [43]. In the α - x plane, the monodisperse case corresponds to the Kepler limit $\alpha = 1$; in this limit, the packing fraction of the densest packings is $\phi = \pi/\sqrt{18} = 0.740480\dots$. This fraction is achieved by any of the infinite number of Barlow packings [44], which include the well-known fcc and hcp sphere packings. Some efforts have been made to identify the densest alloy packings away from the limit $\alpha = 1$ by using simple crystallographic techniques [27,45]; however, these have been limited to only a small subset of possible periodic alloy packings.

Methods such as Monte Carlo [39,46,47] and genetic algorithms [37] have also been employed, with limited success, to attempt to find densest binary sphere packings over certain ranges of α and x . In part due to the enormous number of different initial sphere spatial configurations required by these methods to identify densest packings of a large number of spheres, high resolution searches in α and x would previously have required an enormous amount of computational time. As

a result, the densest alloys found by past efforts were limited to minimal bases with relatively smaller numbers of spheres, and, aside from the XY_n packings, relative compositions of $x = 1/2$, $x = 2/3$, and very recently, $x = 3/4$ [36]. In contrast, employing an implementation of the TJ sphere-packing algorithm [34], we have found several new alloys for $\alpha > \sqrt{2} - 1$ including three with 12, 10, and 7 spheres in their minimal bases in respective small to large number ratios of one to one, seven to three, and five to two.

Using the TJ algorithm, an overview of which is given in Sec. III, we have systematically surveyed the parameter space $(\alpha, x) \in [0, 1] \times [0, 1]$, omitting the rectangular area $\alpha < 0.2$ and $x > 11/12$ for reasons mentioned below, to find the putative densest binary packings at high resolution in α and x for bases of up to 12 spheres. From this survey, we are able to construct the most comprehensive determination to date of the phase diagram of the densest binary packings in \mathbb{R}^3 in the α - x plane and the best-known lower bound on the function $\phi_{\max}(\alpha, x)$ for the values of α that we survey. Though the representation we construct is technically a lower bound on $\phi_{\max}(\alpha, x)$ as it excludes densest aperiodic packings and periodic packings with bases greater than 12, we contend (for reasons described in Sec. III) that for the vast majority of (α, x) , it is a precise representation of $\phi_{\max}(\alpha, x)$.

We present different representations of the most comprehensive determination to date of the phase diagram in Figs. 2, 3, 5, 7, and 14. Similar versions of Figs. 2 and 3 were presented in Ref. [33]. In Fig. 5, we describe heretofore unknown alloys by the number of small and large spheres in their minimal bases, e.g., (6-6) for the alloy with six small and six large spheres. In both figures, phase boundaries are drawn between packings with *distinct* alloys, where each distinct alloy exhibits a unique lattice system characterization of its fundamental cell and composition of spheres in its minimal basis. In the figures, points (lines) where the composition of phase-separated phases changes from alloy plus monodisperse packing of small spheres to the same alloy plus a monodisperse packing of large spheres are not drawn. In Fig. 5, where only one alloy is listed, it is assumed that the densest packing

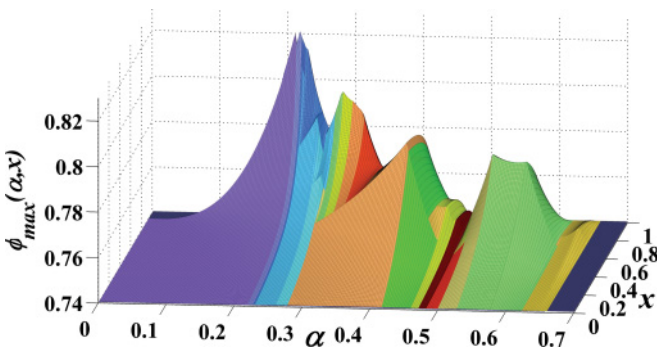


FIG. 2. (Color online) The most comprehensive determination to date of the phase diagram and maximal packing fraction surface $\phi_{\max}(\alpha, x)$ of the densest binary sphere packings in \mathbb{R}^3 . The highest point is $\phi_{\max}(0.224744\dots, 10/11) = 0.824539\dots$, and all packings for approximately $\alpha > 0.660\dots$ consist of two phase-separated monodisperse Barlow phases. Note that we have excluded the rectangular region $\alpha < 0.20$, $x > 11/12$. Different shading indicates a different phase composition, as specified in Fig. 5.

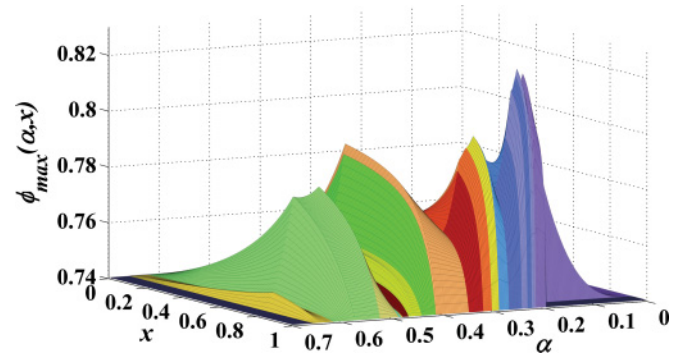


FIG. 3. (Color online) The most comprehensive determination to date of the phase diagram and maximal packing fraction surface $\phi_{\max}(\alpha, x)$ of the densest binary sphere packings in \mathbb{R}^3 . Note that we have excluded the rectangular region $\alpha < 0.20$, $x > 11/12$. Different shading indicates a different phase composition, as specified in Fig. 5.

consists of a monodisperse phase and an alloy phase, except at points such that $x = S_i/(S_i + L_i)$, with S_i and L_i the respective numbers of small and large spheres in the minimal basis of the alloy phase listed, where only the alloy phase is present.

Each distinct alloy appears in the densest packings over a range of α . However, most alloys exhibit varying contact networks over this range, where a contact network describes the numbers of small and large sphere contacts for each sphere in the minimal basis. Each distinct alloy could thus be subdivided into “suballoys” based on contact networks, as was done for the periodic disk alloys in Ref. [38]. Though we do not make these subdivisions in this work due to the very large number of suballoys that would be identified, we note that there are practical reasons for the subdivision. In particular, subdivision by contact network would allow for characterization of all of the line segments in the α - x plane along which the slope of the surface changes discontinuously. These discontinuities can be clearly seen in Fig. 4, plots of the best-known lower bounds on $\phi_{\max}(\alpha, 1/2)$ and $\phi_{\max}(\alpha, 2/3)$ for $0 \leq \alpha \leq 0.7$. In Fig. 4, M_S and M_L refer to monodisperse, Barlow-packed phases of small and large spheres, respectively.

One example of a discontinuity in slope occurring along a line segment inside a phase region is for the highest point in Figs. 2 and 3, at $\phi_{\max}(0.224744\dots, 10/11) = 0.824539\dots$. If this phase region was subdivided according to the contact networks of the alloys that compose the phase, this point would occur along a phase boundary. Another example is found in the alloy with triclinic lattice system characterization with six small spheres and one large sphere in its minimal basis, present in the densest packings over the range $0.292 \leq \alpha \leq 0.344$. In Figs. 2, 3, and 5, to serve as an example, the phase region including this alloy has been subdivided according to the number of large-large sphere contacts in the alloy. There are eight, six, and four large-large sphere contacts, respectively, in the $(6-1)_8$, $(6-1)_6$, and $(6-1)_4$ “suballoys,” and close inspection of the bottom plot in Fig. 4 reveals discontinuous changes in slope in α at each of the boundaries between them.

In general, the surface presented in Figs. 2 and 3 is continuous and piecewise differentiable, though as $\alpha \rightarrow 0$ and $x \rightarrow 1$, the density of curves along which the surface

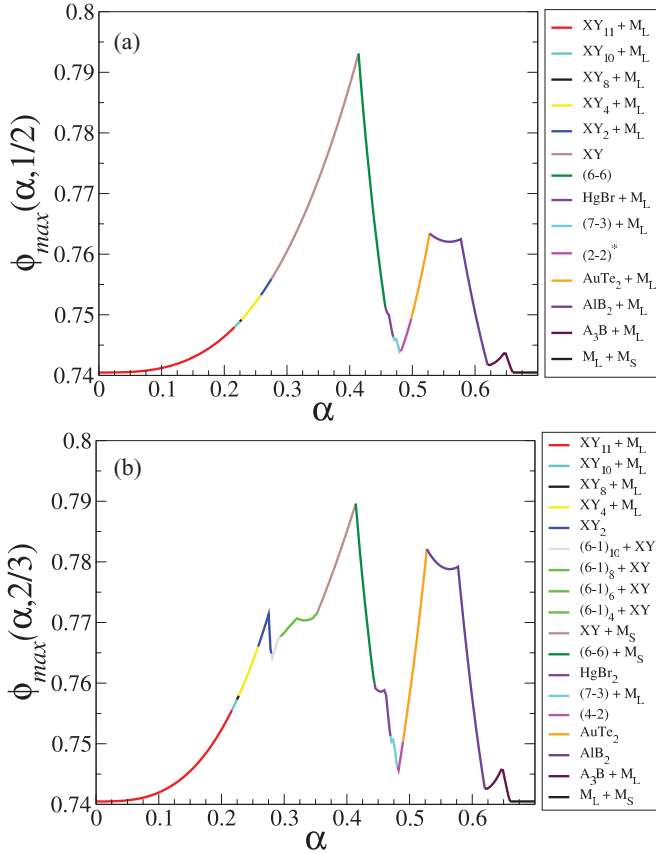


FIG. 4. (Color online) Plots of the best-known lower bounds on $\phi_{\max}(\alpha, x)$ for $0 \leq \alpha \leq 0.7$ and (a) $x = 1/2$, and (b) $x = 2/3$, considering minimal bases up to 12 spheres. Coloration (shading) in these plots indicates the phases present in the densest packings. The different shadings in curves appearing from left to right correspond to shadings in the legend from top to bottom.

is not differentiable approaches infinity due to the number of XY_n and similar packings. For this reason, we exclude the region $\alpha < 0.2$, $x > 11/12$ from our study, truncating α at 0.2 because it is close to the maximum value $\alpha = 0.216633\dots$ at which 11 small spheres fit in the interstices of a close-packed Barlow packing of large spheres. For $\alpha > 0.660\dots$, we have been unable to find any periodic packing with a

basis of 12 or fewer spheres that exceeds the packing fraction $\pi/\sqrt{18}$ of two phase-separated monodisperse Barlow-packed phases.

Away from the point $(\alpha, x) = (0, 1)$, we represent the surface at given α piecewise analytically in x . This is possible because densest packings can be constructed from a finite number of phase-separated alloy and Barlow-packed monodisperse phases, where phase-separated packings are the densest since the interfacial volume of the boundaries between phases is negligible in the infinite volume limit. Further, we prove in Sec. IV that at any point (α, x) with $\alpha > 0$, $x < 1$, there is at least one densest binary packing that consists of no more than two phases. However, this does not preclude the possibility of a densest packing consisting of more than two distinct phases, nor the possibility of ‘‘mixing’’ of phases in certain specific cases where there is no boundary cost.

In Sec. II, differences between periodic, aperiodic, disordered, and quasicrystalline packings are described. We discuss which types of packings are found to be the densest in \mathbb{R}^2 and which we have been able to find (and predict to find) in \mathbb{R}^3 . In Sec. III, an overview of the TJ algorithm is provided that includes reasons why the algorithm is particularly successful in identifying dense alloys. In Sec. IV, we describe precisely the method used to construct the maximal-density surface ϕ_{\max} and present a proof of why for η different sizes of spheres in any dimension d , there is always a densest packing consisting of only η phase-separated phases. In Sec. V, the structural details of the putative densest binary sphere packings in \mathbb{R}^3 for minimal bases of 12 or fewer spheres are presented and their properties discussed. In Sec. VI, we conclude with the goals of related future research and the implications and applications of our findings.

II. PERIODIC PACKINGS, APERIODIC PACKINGS, AND JAMMING

The space of binary sphere packings in \mathbb{R}^d can be formed from a configuration of points where there are N_S points designated type S and N_L points designated type L . Each pair of points of type S must be separated by at least distance $2R_S$, each pair of points of type L by at least a distance $2R_L$, and each pair including one point of each type by at least a distance

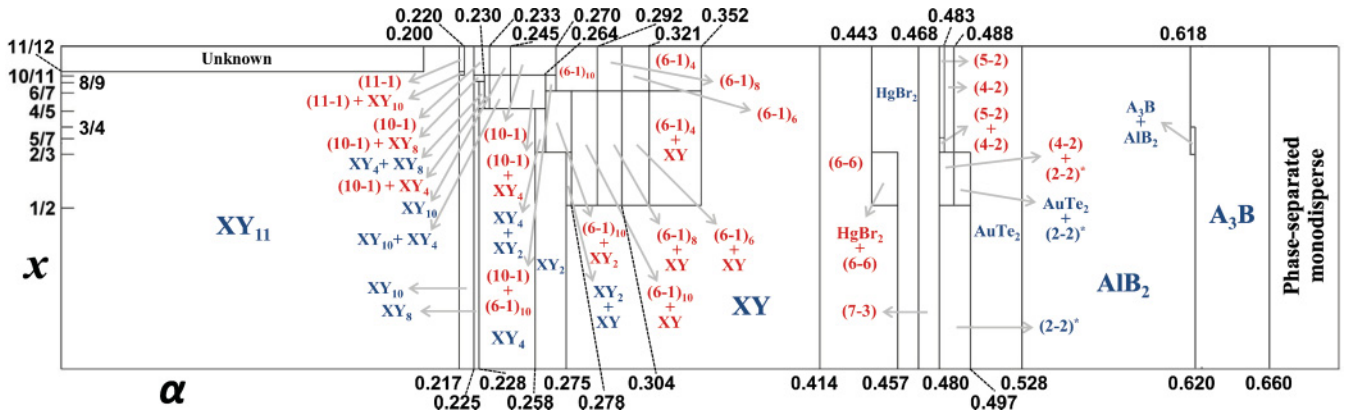


FIG. 5. (Color online) Phase diagram in (α, x) , excluding the region $\alpha < 0.2$ and $x > 11/12$, of the densest-known binary sphere packings in \mathbb{R}^3 considering periodic packings with minimal bases of 12 or fewer spheres. Figures 7 and 14 are larger versions of this image.

$R_S + R_L$. With the points representing sphere centers, this construct describes the space of all binary packings of small (S) and large (L) spheres in \mathbb{R}^d with radius ratio $\alpha = R_S/R_L$ and small sphere relative concentration $x = N_S/(N_S + N_L)$.

Configurations of points can be categorized by their spatial distributions. In this way, all packings can be described as lattice, periodic, or aperiodic. A *lattice* Λ in \mathbb{R}^d is a subgroup consisting of the integer linear combinations of a given set of d *lattice vectors* that span \mathbb{R}^d . This is referred to as a *Bravais lattice* in the physical sciences and engineering. A *lattice packing* of identical nonoverlapping objects is one in which the objects have centers located at the points of Λ . In a lattice packing, the space \mathbb{R}^d can be geometrically divided into identical regions called *fundamental cells*, each of which contains the center of only one object. For a lattice packing of spheres, which are necessarily identical, the packing fraction ϕ in \mathbb{R}^d is given by

$$\phi = v_1(R)/V_F, \quad (2)$$

with R the radius of the spheres, V_F the volume of the fundamental cell, and

$$v_1(R) = \pi^{d/2} R^d / \Gamma(1 + d/2) \quad (3)$$

the volume of a single sphere, where $\Gamma(x)$ is the Euler Γ function.

An extension of the notion of a lattice packing is a *periodic packing*. A periodic packing is obtained by placing a fixed configuration of the centers of $N \geq 1$ objects, called the *basis*, in one cell of a lattice Λ , and then replicating this fixed configuration, without overlap, in all other cells. The cell in this case is termed a *unit cell*, and is also a fundamental cell with corresponding *minimal basis* if and only if no smaller unit cell (with fewer than N object centers) can describe the same packing. In either case, the packing fraction for a packing of spheres, not necessarily identical in size, is given by

$$\phi = \frac{\sum_{i=1}^N v_1(R_i)}{V_U}, \quad (4)$$

with R_i the radius of each sphere in the basis and V_U the volume of the cell. It is critical to note that no binary packing with $0 < x < 1$ can be a lattice packing, since the basis of a binary packing, by definition, must consist of at least two objects.

An aperiodic packing is one that exhibits no long-range translational order; *i.e.*, its minimal basis is equal to the number of particles in the packing. Practically speaking though, a packing with a very large number of objects might be called aperiodic if it is comprised of only a few translations of the minimal basis. Both periodic and aperiodic structures are found widely in nature; examples of the former include crystalline solids like many metals and salts, and examples of the latter include liquids, glasses, gels, gases, plasmas, and quasicrystals [48].

A quasicrystal is an aperiodic structure that nonetheless exhibits bond orientational order in symmetries (e.g., fivefold) forbidden to periodic crystals. We refer the reader to Ref. [49] for a more precise definition. We describe a *directionally periodic* structure as an aperiodic structure that exhibits a

period along at least one spatial axis but never simultaneously along d lattice vectors, *e.g.*, a random stacking Barlow packing.

The Barlow packings are constructed by stacking layers, each consisting of contacting spheres in \mathbb{R}^3 with centers on a plane in a triangular lattice configuration, on top of one another. There are two ways (layers in positions B and C) to stack such a layer on top of another (layer in position A) such that all spheres in each layer are in contact with three spheres in the adjacent layer. Any packing that is composed of an infinite number of A , B , and C layers, with no adjacent layers the same, is a Barlow packing and achieves the maximal packing fraction of identical spheres in \mathbb{R}^3 . A random stacking of layers according to these rules is a random stacking Barlow packing, which exhibits periodicity parallel to the planes of the layers but not perpendicular to them.

For the purposes of this paper, we describe a *disordered* structure as an aperiodic structure that does not exhibit perfect long-range symmetry, translational, rotational, or reflective, of any kind.

In \mathbb{R}^2 , periodic, quasicrystalline, and directionally periodic structures can all be found among the putative densest binary disk packings [38,50–52]. We believe that all of these types of structures may be found among the densest binary sphere packings in \mathbb{R}^3 as well, though we have identified only periodic and directionally periodic structures in this work. Due to computational constraints attributable in large part to the scope and resolution of our survey in (α, x) , we have limited our survey in this work to investigating the densest periodic packings with bases of 12 spheres or fewer. This limitation substantially increases the difficulty of identifying aperiodic packings, which most often cannot be approximated well by a fundamental cell with a basis of only 12 spheres, though densest directionally periodic packings often can still be identified by extrapolating from periodic packings.

One property of a densest packing is that a subset of its objects is *collectively jammed* or, in the case of a densest periodic packing, that the objects within each unit cell are *strictly jammed* under periodic boundary conditions. None of the nonoverlapping objects in a packing that is *locally jammed* can be continuously displaced (displaced by infinitesimally small movements) without displacing one of its neighbors [53]. In a collectively jammed packing, a subset of the objects (the *backbone*) is locally jammed and no continuous collective motion of any subset of objects can lead to *unjamming*, *i.e.*, a packing that is no longer locally jammed. The objects that can be displaced without displacing their neighbors in a collectively jammed packing are termed *rattlers*. A strictly jammed packing is collectively jammed, and no collective motion of any subset of objects, coupled with a continuous spatially uniform deformation of the boundary that does not increase volume, can result in unjamming. If a subset of the objects in a packing is not collectively or strictly jammed, then, by definition, a uniform continuous motion exists that results in free space around the objects, *i.e.*, the packing is not a densest packing because its volume can be reduced.

One reason that the TJ algorithm is particularly effective at finding densest periodic packings is that it guarantees that final packings are strictly jammed [34]. If there is a

collective continuous motion of the spheres, coupled with a uniform continuous deformation of the unit cell, that will decrease the volume of the cell, then the exact linear programming method employed by the TJ algorithm will find that motion.

With respect to jamming, a certain group of packings that we call “host-guest” packings deserves further attention. In such a packing, a subset (usually the larger spheres) of the total packing is packed as a jammed periodic packing, and a mutually exclusive subset (usually the smaller spheres) sits in the interstices formed by the jammed spheres but without contacting the jammed spheres. Clearly, the spheres within the interstices can be continually displaced without altering the density of the packing. In this way, a host-guest packing can be periodic or aperiodic. If the rattlers are placed in the same place relative to one another throughout every cell of the packing, then the packing is periodic. If they are placed at random, then the packing is aperiodic. A host-guest packing is similar in nature to an interstitial solid solution (ISS) phase, such as the stable binary colloidal phases described in Ref. [54]. We are not aware of any densest packings where the large spheres are free to move, as rattlers, within interstices created by jammed small spheres.

The XY_n packings where small spheres are not required to contact the jammed large spheres are good examples of host-guest sphere packings, where an XY_n packing consists of a Barlow-packed structure of contacting large spheres with small spheres placed in the interstices. Among the host-guest packings, one can distinguish topologically between packings where the small spheres are small enough to move freely about all of the interstices and packings where they are confined to a given interstice or finite set of interstices. In the former case, the space available to the small spheres is topologically connected, where in the latter case it is not. Though we find densest packings (e.g., XY_n packings) where small spheres are confined to a single interstice, we do not find for $\alpha \geq 0.2$ any case where they are free to move about all of the interstices. However, it is the case for small enough α that there are densest host-guest packings where the space available to the small spheres is topologically connected.

III. THE TORQUATO-JIAO SPHERE-PACKING ALGORITHM

There are several factors that have limited past algorithmic techniques in finding densest packings. As previously discussed, one of these is the immensity of the parameter space in (α, x) of densest binary packings. Another is the strong initial condition dependence of many algorithms, which requires that a very large number of simulations beginning with different initial spatial conditions be undertaken to find a densest packing. This required number of simulations can increase exponentially with the number of spheres simulated.

Past algorithmic techniques have also been limited by the vast multitude of local minima in “energy,” defined as the negative of the packing fraction, present in the phase space of a periodic sphere packing with unit cell of indeterminate size and shape with even a small basis. Methods that move only one sphere at a time cannot escape from local minima where a collective motion of spheres is required to decrease energy, and

methods that move several spheres at once rely on chance, and hence a very large number of steps, to find the right collective movement. Many molecular dynamics algorithms rely upon principles of equilibrium thermodynamics, which necessitate that large numbers of time-consuming steps (individual sphere movements) be taken at each stage of sphere growth or compression of the unit cell in order to reduce the chance of becoming “stuck” in a local minimum.

In this paper, we are able to overcome these time and computational limitations by using the TJ linear programming algorithm [34]. The TJ sphere-packing algorithm does not easily become stuck in local minima because it is inherently designed to find the simultaneous collective linear motion of both the spheres and the unit cell geometry that maximizes the density of the packing.

The TJ algorithm approaches the problem of generating dense, periodic packings of nonoverlapping spheres with an arbitrary size distribution as an optimization problem to be solved using linear programming techniques. In particular, the objective function is chosen to be the negative of the packing fraction (as indicated above), which is minimized with respect to particle (sphere center) positions and the shape and size of the unit cell, subject to sphere nonoverlap conditions. The use of a deformable unit cell, defined in terms of d , d -dimensional lattice vectors $\mathbf{M}_\Lambda = \{\lambda_1; \dots; \lambda_d\}$, was first introduced by Torquato and Jiao [16] to obtain dense packings of hard polyhedral particles including Platonic and Archimedean solids.

For nonoverlapping spheres, the optimization problem can be efficiently solved by linearizing the objective function and nonoverlap constraints. This approach has the advantage of being rigorously exact near the jamming limit of the spheres and unit cell [34].

The TJ algorithm begins with an initial packing of N spheres, and obtains a new, denser packing by solving the following linear programming problem:

$$\begin{aligned} \text{minimize: } & \text{Tr}(\boldsymbol{\varepsilon}) = \varepsilon_{11} + \dots + \varepsilon_{dd} \\ \text{subject to: } & \mathbf{M}_\Lambda \cdot \mathbf{r}_{ij}^\lambda \cdot \boldsymbol{\varepsilon} \cdot \mathbf{M}_\Lambda \cdot \mathbf{r}_{ij}^\lambda + \Delta \mathbf{r}_{ij}^\lambda \cdot \mathbf{G} \cdot \mathbf{r}_{ij}^\lambda \\ & \geq \frac{1}{2}(\overline{D}_{ij}^2 - \mathbf{r}_{ij}^\lambda \cdot \mathbf{G} \cdot \mathbf{r}_{ij}^\lambda) + \mathcal{R}, \end{aligned}$$

for all neighbor pairs (i, j) of interest, and

$$\begin{aligned} \Delta \mathbf{x}_i^{\lambda, \text{lower}} \leq \Delta \mathbf{x}_i^\lambda \leq \Delta \mathbf{x}_i^{\lambda, \text{upper}}, \quad \forall i = (1, \dots, N), \\ \varepsilon_{kl}^{\text{lower}} \leq \varepsilon_{kl} \leq \varepsilon_{kl}^{\text{upper}}, \quad \forall k, l = (1, \dots, d), \end{aligned} \quad (5)$$

where $\overline{D}_{ij} = (D_i + D_j)/2$ is the average diameter of spheres i and j ; $\mathbf{r}_{ij}^\lambda = \mathbf{x}_i^\lambda - \mathbf{x}_j^\lambda$ is the displacement vector between spheres i and j in the initial packing with respect to the lattice vectors \mathbf{M}_Λ ; $\Delta \mathbf{r}_{ij}^\lambda = \Delta \mathbf{x}_i^\lambda - \Delta \mathbf{x}_j^\lambda$ is the relative change in displacement of spheres i and j in coordinates with respect to the \mathbf{M}_Λ ; $\boldsymbol{\varepsilon} = \{\varepsilon_{kl}\}$ is the strain tensor associated with the unit cell, with lower and upper bounds $\{\varepsilon_{kl}^{\text{lower}}\}$ and $\{\varepsilon_{kl}^{\text{upper}}\}$, respectively; $\mathbf{G} = \mathbf{M}_\Lambda^T \cdot \mathbf{M}_\Lambda$ is the *Gram matrix* of the lattice; and \mathcal{R} is a scalar representing higher order terms, which are given in Appendix A. The *neighbor* pairs are determined by an *influence sphere* with radius γ_{ij} , i.e., two spheres i and j are considered neighbors if their pair distance is smaller than γ_{ij} . We note that the choice of the influence sphere radius can significantly affect the density and degree of disorder in the

final packing. For densest packings, a large γ_{ij} should be used, as detailed in Ref. [34]. We also note that to study packings of spheres with nonadditive diameters, one simply sets \bar{D}_{ij} to the desired value when spheres i and j are not of the same type.

Our tests of the TJ algorithm, for which the implementation for binary sphere packings is described in Appendix A, indicate that the algorithm is both particularly efficient and particularly robust in finding densest packings across the entire range of (α, x) for a sufficiently small basis of spheres. For example, we have recovered all of the alloys known to be present in the densest packings, including the A₃B [36], AlB₂, HgBr₂, AuTe₂, and “Structure 2” [39] alloys, and XY_{*n*} packings for certain values of n . In addition, we have found many areas in the α - x plane where the densest packings are denser than previously predicted and include heretofore unknown alloys. Overall, in the area of the α - x plane searched, we always recover a packing fraction $\phi_{\max}(\alpha, x)$ that is either greater than or equal to that previously known.

IV. IDENTIFYING THE DENSEST BINARY SPHERE PACKINGS

To identify the densest binary packings in \mathbb{R}^3 , we begin with the obvious statement that at all given (α, x) , there is a densest packing that consists of a finite number of phase-separated alloy and monodisperse phases. In the infinite volume limit in \mathbb{R}^d for η different sizes of spheres, the packing fraction of a phase-separated collection of β monodisperse and distinct alloy phases can be written

$$\phi = \frac{[\pi^{d/2}\Gamma(1+d/2)]\left[\sum_{j=1}^{\eta} X^{(j)}(R^{(j)})^d\right]}{\sum_{i=1}^{\beta} \frac{C_i}{S_i^{F_i}} x_i^{F_i}}, \quad (6)$$

with $X^{(j)}$ and $R^{(j)}$ the relative fraction and radii, respectively, of spheres of type (size) j , x_i^j the relative fraction of spheres of type j distributed in phase i ($\sum_{i=1}^{\beta} x_i^j = X^{(j)}$), and C_i the volume of a unit cell of phase i containing, for each sphere type j , S_i^j spheres. The index $j = F_i$ in $S_i^{F_i}$ and $x_i^{F_i}$ is the first index j in phase i such that $S_i^j \neq 0$. For η sphere sizes, there are η monodisperse phases with relative fraction $x_i^{F_i}$, $F_i = 1, \dots, \eta$, respectively, and $S_i^j = 0$ for all $j \neq F_i$, representing packings with spheres packed as densely as possible in \mathbb{R}^d .

To find the densest packing $\phi_{\max}(R^{(1)}, \dots, R^{(\eta)}, X^{(1)}, \dots, X^{(\eta)})$ at specified sphere sizes $R^{(j)}$ and relative compositions $X^{(j)}$ from among β known alloy and close-packed monodisperse phases, Eq. (6) must be maximized. This is accomplished by minimizing the denominator of Eq. (6) over the relative fractions $x_i^{F_i}$. As the denominator is linear in the variables $x_i^{F_i}$, it can be formulated as the objective function in a linear programming problem. This formulation allows us to state the following theorem, the proof of which is found in Appendix B. We note that Theorem 1 applies not only to spheres, but in fact to any packing of η different types of objects in \mathbb{R}^d with specified volumes and relative fractions $X^{(j)}$.

Theorem 1. Consider any sphere packing in \mathbb{R}^d composed of β phase-separated alloy and monodisperse phases. For η different sizes of spheres, there is always a densest packing consisting of no more than η phase-separated phases.

For binary sphere packings with $\eta = 2$ in \mathbb{R}^3 , it is thus clear that there is at least one densest packing at every (α, x) consisting of no more than two phases. For simplicity in this case, we set $X^{(1)} = 1 - x$ to be the relative fraction of large spheres and $X^{(2)} = x$ the relative fraction of small spheres, and we rewrite Eq. (6) as

$$\phi = \frac{\frac{4\pi}{3}[(1-x)R_L^3 + xR_S^3]}{xC_B^S + (1-x)C_B^L + \sum_{i=1}^{\beta} x_i^L \left(\frac{C_i}{L_i} - \frac{S_i}{L_i} C_B^S - C_B^L\right)}, \quad (7)$$

with C_B^S and C_B^L the volume per sphere, respectively, in a close-packed Barlow packing of small and large spheres, x_i^L the relative fraction of large spheres distributed in alloy phase i , and C_i the volume of a fundamental cell of alloy phase i containing L_i large and S_i small spheres.

Using Eq. (7) and considering a fixed value of α , the densest binary packings in \mathbb{R}^3 can be found for all values of x by solving for all globally optimal vertices considering all dense alloy phases at α . Since we limit ourselves in this work to minimal bases of no more than 12 spheres, we must assume that all of these alloy phases can be constructed from repetitions of local structures consisting of 12 spheres or fewer. Though we recognize that this assumption is most likely false for some values of α , especially near the point $(\alpha, x) = (0, 1)$, we contend that for the majority of the area of the parameter space studied, it is correct. We therefore employ the TJ algorithm to search the space of fundamental cells in \mathbb{R}^3 containing all combinations of positive integer L_i and S_i such that $L_i + S_i = 2, 3, \dots, 12$. We have solved these problems (putatively) to an accuracy of about 10^{-4} in ϕ for α spaced 0.025 apart and on a finer grid with α spaced about 0.0028 apart for certain values of S_i and L_i where particularly dense packings were identified.

V. PACKING RESULTS

In the following sections, the densest binary sphere packings that we have identified employing the TJ algorithm are presented. In Table I of Appendix C, we list packing fractions for those alloys about which we were unable to find descriptions in the literature. For each of these alloys, packing fractions are listed only over the range of α where the alloy appears in the densest packings. In Sec. V A, we discuss some of the properties of these packings, including, for example, the lattice symmetry of alloy phases present in the packings and classification of these phases as periodic or aperiodic. The properties that we discuss do not serve as an exhaustive list, nor are the examples we provide the only examples of densest binary packings with these properties. Instead, we discuss packing properties with the intent of providing an overview of the diversity of the different types of densest packings.

The figures presented in this section are illustrations of unit cells of the alloys that appear in the densest packings, where the unit cells are chosen to highlight packing symmetry. Contacts between two large spheres are indicated by dotted lines, as are contacts between two small spheres; however, large-small contacts are not drawn. Unit cell boundaries are also indicated by dotted lines, and unit cell boundary lengths are displayed

in units of the diameter of the large spheres. Angles are given in degrees.

A. Packing properties

The densest binary sphere packings that we have identified exhibit a broad array of properties. For example, there are densest packings that consist of only a single phase and many that consist of multiple phases. In the majority of these phases, all spheres are collectively jammed. In others, each fundamental cell contains rattlers; that is, there are an infinite number of sphere configurations in each cell that exhibit the same packing fraction. In others still, there are only a finite number of sphere configurations in each cell that exhibit identical packing fraction.

Concerning rattlers in densest packings, it is intuitive that for the majority of the volume of the parameter space of densest packings of η different sizes of spheres, packings with rattlers would dominate as η increases. This is because for densest packings with substantial size disparity between the largest and smallest spheres, except for at selected values of X^j , it seems clear that the small spheres would move about as rattlers in the interstices formed by jammed larger spheres. It is interesting therefore that we have found that there are densest binary packings over the majority of the α - x plane that are composed of phases that do not include rattlers.

For the rectangular region $\alpha < 0.2$, $x > 11/12$, we have not attempted to identify densest packings. This is because the number of distinct densest packings, for example, those of type XY_n , approaches infinity as $\alpha \rightarrow 0$ with $x \rightarrow 1$. In this latter limit, the densest packings are the XY_∞ packings consisting of infinitesimally small Barlow-packed small spheres located within the spaces between Barlow-packed large spheres. The packing fraction of this packing is [8]

$$\lim_{(\alpha,x) \rightarrow (0,1)} \phi_{\max}(\alpha,x) = 1 - (1 - \pi/\sqrt{18})^2 = 0.932\,649\dots \quad (8)$$

At all points (α,x) outside of the rectangular region $\alpha < 0.2$, $x > 11/12$, we have identified putatively densest packings that consist only of periodic alloy phases. However, due to the infinity of densest Barlow packings (which are, in general, directionally periodic), all densest packings that contain a periodic monodisperse phase are degenerate in density with packings exhibiting an aperiodic monodisperse phase. Additionally, there are alloys that can be paired with monodisperse Barlow packings without a boundary cost, *e.g.*, the AIB_2 alloy. This pairing allows a “mixed-phase” densest packing, or a densest packing composed of a single aperiodic (directionally periodic) phase. There are also pairs of alloys that appear to exhibit this property.

For the majority of the area in the α - x plane, the densest packings consist of two phase-separated phases, one alloy and one monodisperse. For $\alpha > \alpha^* \approx 0.660$, the known densest binary packings consist simply of two phase-separated monodisperse Barlow-packed phases. For $(\alpha,x) \in (0,\alpha^*) \times (0,1)$, either a single alloy phase or a combination of an alloy and a monodisperse phase is known to be denser than two phase-separated monodisperse phases.

At certain points, densest packings consisting of three distinct phases can exist. Examples of this case include; at $\alpha = \alpha^*$, $0 < x < 1$, where two monodisperse phases and one A_3B phase exhibit packing fraction $\pi/\sqrt{18}$; at about $\alpha = 0.292$, $6/7 < x < 1$, where one monodisperse (small spheres), one $(6-1)_{10}$, and one $(6-1)_8$ phase exhibit a peak packing fraction of about 0.801; and at the same α with $1/2 < x < 6/7$, where one $(6-1)_{10}$, one $(6-1)_8$, and one XY phase exhibit a peak packing fraction of about 0.801. One example of a packing with four distinct phases occurs at about $\alpha = 0.480$, $1/2 < x < 2/3$, where one monodisperse (large spheres), one $(7-3)$, one $AuTe_2$, and one $(2-2)^*$ phase exhibit a peak packing fraction of 0.748.

B. Densest packings for $\alpha \leq \sqrt{2} - 1$

Many of the densest binary alloys for $\alpha < \sqrt{2} - 1$ are of the XY_n type. In an XY_n alloy, the small spheres, of which there are n for every large sphere, are distributed in the octahedral and sometimes tetrahedral interstices, of which there are one and two, respectively, for each strictly jammed Barlow-packed large sphere. The XY_n alloys are present in the densest binary packings that we have found for $n = 1, 2, 4, 8, 10$, and 11 . In these packings, the small spheres occupy the interstices as rattlers, except for “magic” [38] α , where they are jammed between large spheres, *e.g.*, at $\alpha = \sqrt{2} - 1$ for the NaCl alloy. All XY_n alloys belong to the cubic lattice system.

For $n = 1, 2, 4$, and 8 , these small spheres occupy only the octahedral interstice, where for $n = 4$ and $n = 8$, each set of 4 and 8 spheres in an interstice at the “magic” radii form a perfect tetrahedron and cube, respectively. For $n = 10$, a small sphere occupies each of the tetrahedral interstices, and at the magic radius the remainder form a perfect cube; for $n = 11$, there is one extra small sphere in the cube’s center. Additionally, for $n = 2, 4, 8$, and 10 , there are XY_n alloys for α greater than the magic radius ratios. These packings consist of large spheres arranged as in a Barlow packing (with cubic symmetry) but not in contact, with interstitial jammed small spheres arranged as was the case for the magic α .

In the case of XY_n packings where the large spheres are in contact, it is clear that there is no boundary cost between monodisperse layers of contacting spheres packed in a triangular lattice (which we recall is one layer of a Barlow packing) and an XY_n packing. Furthermore, for $x < n/(n+1)$, different numbers of small spheres can be distributed among the interstices of the Barlow-packed large spheres. Consequently, wherever a densest packing consists of any XY_n phase and a Barlow-packed monodisperse phase of large spheres, mixed phase packings and aperiodic alloy phase packings are also densest packings.

The $(11-1)$ and $(10-1)$ alloys are similar to the XY_{11} and XY_{10} alloys, respectively, except that they belong to the tetragonal and rhombohedral lattice systems. The unit cells of these packings can be viewed respectively as “stretched” and “skewed” versions of the XY_{11} and XY_{10} unit cells, and the packings of large spheres can be seen this way as well. However, the clusters of contacting small spheres that occupy the octahedral interstices in these packings do not stretch and skew in the same fashion as the large spheres. Figures 6 and 8 are images that highlight the symmetry present in these alloys.

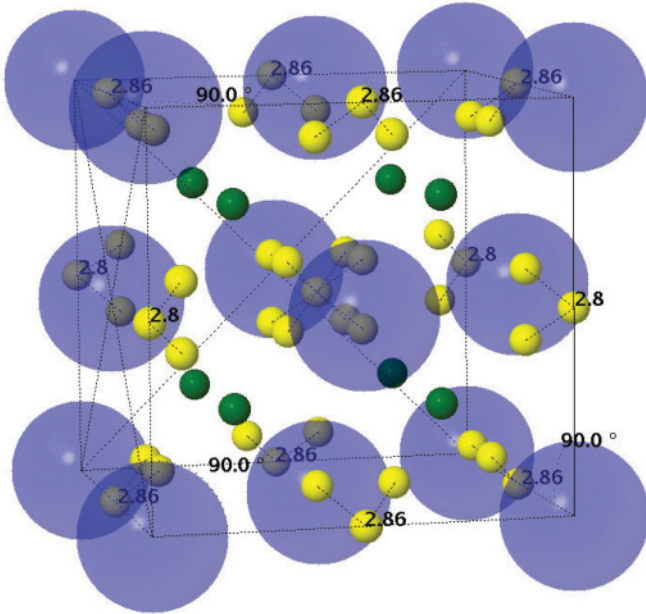


FIG. 6. (Color online) Putative densest packing ($\phi = 0.818$) at radius ratio $\alpha = 0.2195$ of 11 small spheres and 1 large sphere in a periodic fundamental cell. In this image, small spheres in tetrahedral interstices are shown in green (dark gray) and small spheres in octahedral interstices are shown in yellow (light gray). The fundamental cell of this (11-1) alloy belongs to the tetragonal lattice system.

The $(6-1)_{10}$ alloy can be described as a body-centered orthorhombic packing of large spheres with four small spheres present on each of the faces. The small spheres on each face are not in contact, and they are not equidistant from one another owing to the different lengths of the three lattice vectors

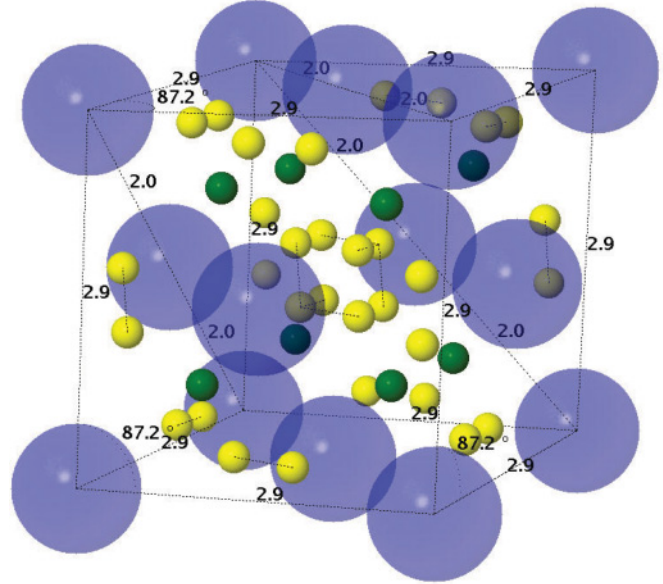


FIG. 8. (Color online) Putative densest packing ($\phi = 0.797$) at radius ratio $\alpha = 0.2503$ of ten small spheres and one large sphere in a periodic fundamental cell. In this image, small spheres in tetrahedral interstices are shown in green (dark gray) and small spheres in octahedral interstices are shown in yellow (light gray). The $(10-1)$ alloy belongs to the rhombohedral lattice system.

comprising the orthorhombic unit cell. Figure 9 illustrates the lack of contact between small spheres, in that the distances depicted between small spheres are all greater than $2\alpha = 0.5562$ large sphere radii. In Fig. 9, the central large sphere contacts all surrounding spheres and the central large spheres in the adjacent unit cells on the z axis, where the z axis is along the basis vectors that are 2.0000 sphere diameters in length.

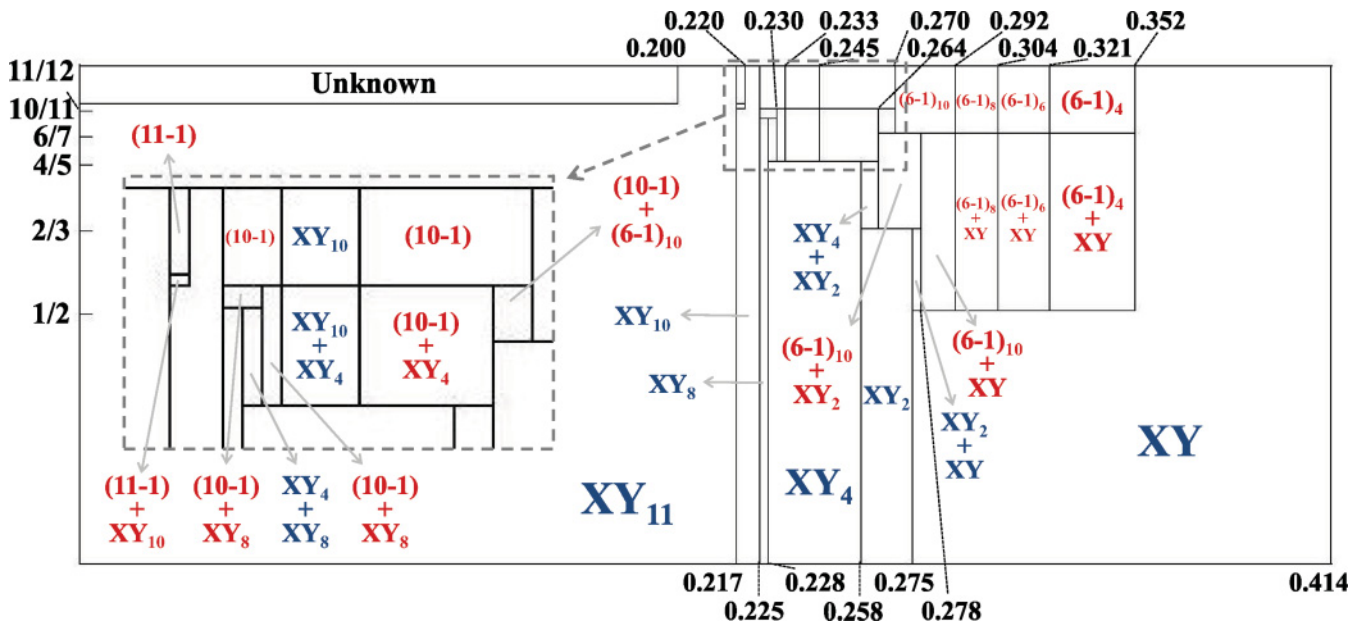


FIG. 7. (Color online) Phase diagram in (α, x) for $0 \leq \alpha \leq \sqrt{2} - 1$, excluding the region $\alpha < 0.2$ and $x > 11/12$, of the densest-known binary sphere packings in \mathbb{R}^3 considering periodic packings with minimal bases of 12 or fewer spheres. This image is an enlargement of the left hand side of Fig. 5.

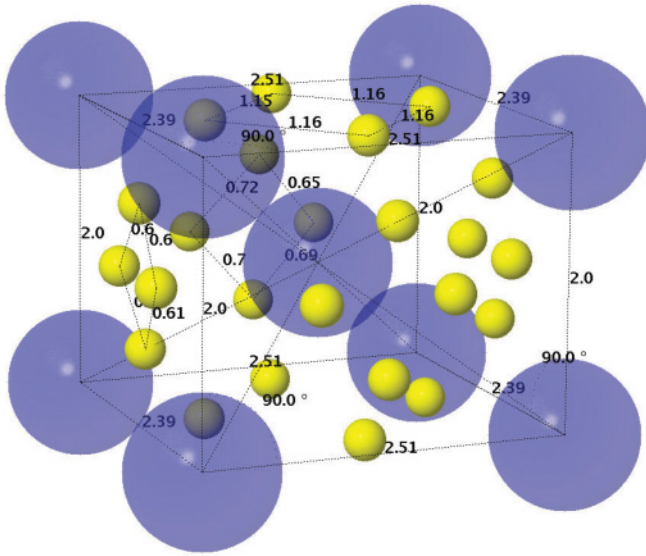


FIG. 9. (Color online) Putative densest packing ($\phi = 0.789$) at radius ratio $\alpha = 0.2781$ of six small spheres and one large sphere in a periodic fundamental cell. In this image, dotted lines between small spheres are drawn to indicate distances and do not indicate contacts. The $(6-1)_{10}$ alloy belongs to the orthorhombic lattice system.

The $(6-1)_8$, $(6-1)_6$, and $(6-1)_4$ suballoys are a subdivision of the alloy exhibiting triclinic lattice system characterization with six small and one large spheres in its minimal basis. This alloy is present in the densest packings over the approximate range $0.292 \leq \alpha \leq 0.352$, and it is very similar to the $(6-1)_{10}$ alloy. Figures 10–12 illustrate large-large and small-small sphere contacts in the $(6-1)_8$, $(6-1)_6$, and $(6-1)_4$ suballoys, respectively. The small spheres in the $(6-1)_8$ suballoy do not contact one another, though many of those in the $(6-1)_6$ and

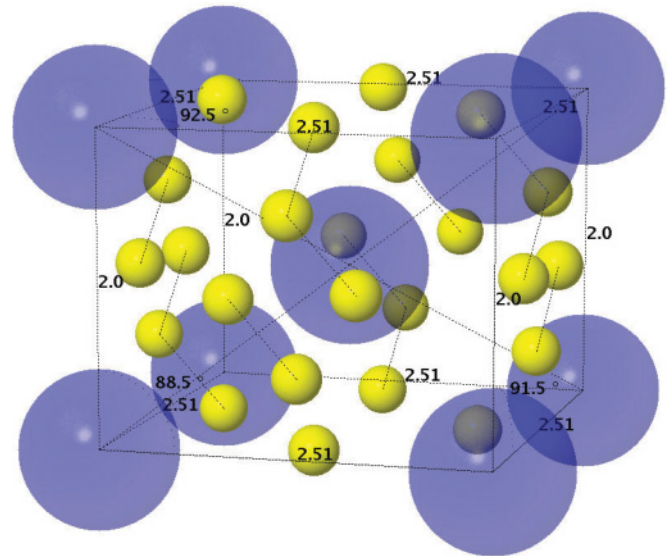


FIG. 11. (Color online) Putative densest packing ($\phi = 0.794$) at radius ratio $\alpha = 0.3151$ of six small spheres and one large sphere in a periodic fundamental cell. The $(6-1)_6$ suballoy belongs to the triclinic lattice system.

$(6-1)_4$ alloys do. Additionally, the centers of the small spheres in the $(6-1)_4$ alloy do not lie on the faces of the triclinic unit cell.

It is also the case that over the entire range that the $(6-1)$ alloys are present in the densest packings they can form mixed phase packings with large spheres packed as in a Barlow packing or with large spheres packed as in a Barlow packing with one small sphere (a rattler) in the octahedral interstice. These mixed phase packings exhibit only slightly smaller packing fractions than their phase-separated counterparts. This is possible due to the nearly cubic symmetry of the $(6-1)$ packings, which allows only a small boundary cost between a $(6-1)$ unit cell and a Barlow-packed unit cell.

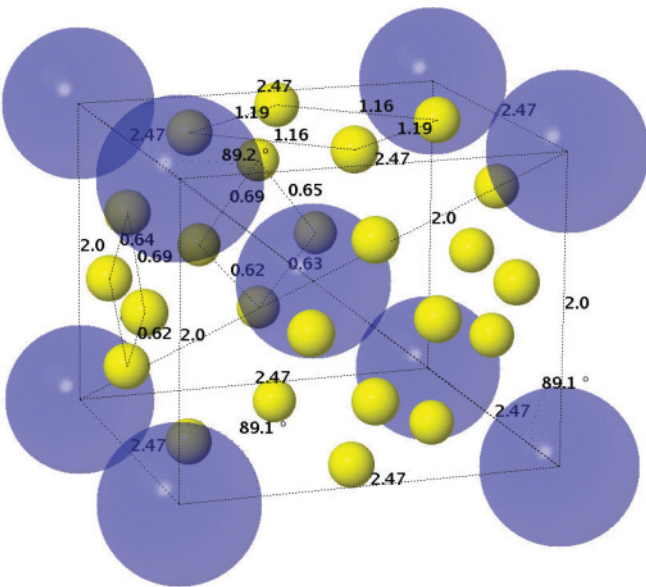


FIG. 10. (Color online) Putative densest packing ($\phi = 0.799$) at radius ratio $\alpha = 0.2980$ of six small spheres and one large sphere in a periodic fundamental cell. In this image, dotted lines between small spheres are drawn to indicate distances and do not indicate contacts. The $(6-1)_8$ suballoy belongs to the triclinic lattice system.

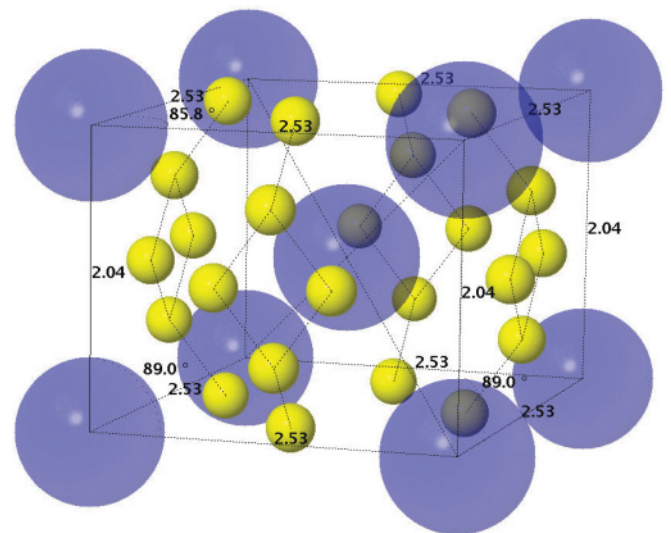


FIG. 12. (Color online) Putative densest packing ($\phi = 0.783$) at radius ratio $\alpha = 0.3293$ of six small spheres and one large sphere in a periodic fundamental cell. The $(6-1)_4$ suballoy belongs to the triclinic lattice system.

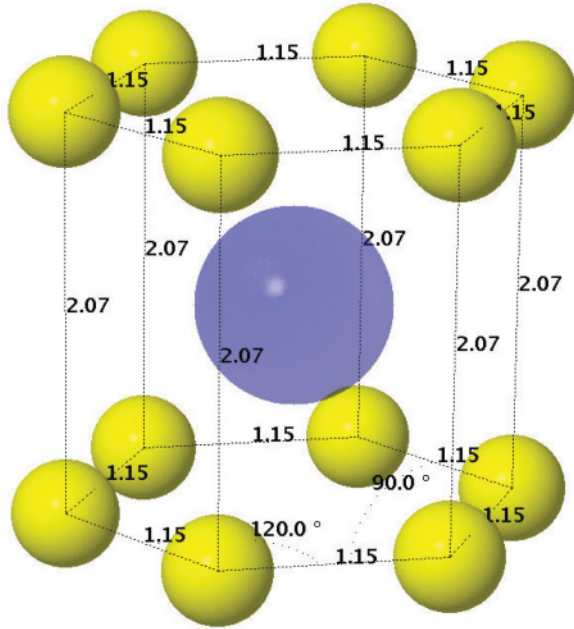


FIG. 13. (Color online) Putative densest packing ($\phi = 0.7793$) at radius ratio $\alpha = 0.5500$ of two small spheres and one large sphere in a periodic fundamental cell. The A_1B_2 alloy belongs to the hexagonal lattice system.

C. Densest packings for $\alpha > \sqrt{2} - 1$

The previously known densest alloys for $\alpha > \sqrt{2} - 1$ all exhibit ratios of small to large spheres of either one to one or two to one. Perhaps the best known is the A_1B_2 alloy (Fig. 13), with two small and one large spheres in its minimal basis, present in the densest packings over the range $\sqrt{7/3} - 1 \leq \alpha \leq 0.620$. This alloy phase can be described as alternating layers of contacting small spheres packed in a honeycomb lattice and large spheres packed in a triangular lattice. The alloy exhibits two maxima in packing density, one at $\alpha = \sqrt{7/3} - 1$ and the other at $\alpha = 1/\sqrt{3}$, with $\phi_{\max}(\sqrt{7/3} - 1, 2/3) = 0.782112\dots$ and $\phi_{\max}(1/\sqrt{3}, 2/3) =$

$0.779205\dots$ At both maxima, the large spheres are in contact both parallel and perpendicular to the planes of the layers.

The $HgBr_2$ alloy was recently discovered to be present in the densest packings [37], a finding that our results support. The alloy phase belongs to the orthorhombic lattice system, and its minimal basis is composed of four small and two large spheres. It exhibits many local maxima and minima in packing fraction over the approximate range $0.443 \leq \alpha \leq 0.468$ that it appears in the densest packings, suggesting that its contact network changes many times over this range. Due to these many local extrema, the packing fraction of the pure $HgBr_2$ alloy phase does not vary much, with $0.752 \leq \phi_{\max}(\alpha, 2/3) \leq 0.760$ over the aforementioned range in α . Figure 15 highlights the large-large and small-small sphere contacts in the alloy at $\alpha = 0.4597$.

The $AuTe_2$ alloy was also recently discovered to be present in the densest packings [37]. The alloy phase belongs to the monoclinic lattice system, and its minimal basis is composed of two small spheres and one large sphere. In a previous work [33], our phase diagram indicated that this alloy was present in the densest packings over the approximate range $0.480 \leq \alpha \leq 0.528$, the same range that was reported in Ref. [37]. However, we correct this statement to read that the alloy appears to be present in the densest packings over the range $0.488 \leq \alpha \leq 0.528$, with the (4-2) alloy present over the approximate range $0.480 \leq \alpha \leq 0.488$. Figure 16 highlights the large-large and small-small sphere contacts in the $AuTe_2$ alloy at $\alpha = 0.4995$.

The A_3B alloy was recently discovered [36] to be the densest-known binary alloy over the approximate range $0.619 < \alpha < \alpha^*$. Previously, the A_1B_2 alloy was thought to be the only alloy denser than phase-separated monodisperse small and large spheres for high enough α , where it becomes less dense than a phase-separated monodisperse packing for all $\alpha > 0.623387\dots$ The fundamental cell of the A_3B alloy, depicted in Fig. 17, belongs to the orthorhombic lattice system, and it contains six small and two large spheres.

In our investigations, the (2-2)* alloy exhibits the same packing fraction (error of less than 10^{-4}) as the Structure 2

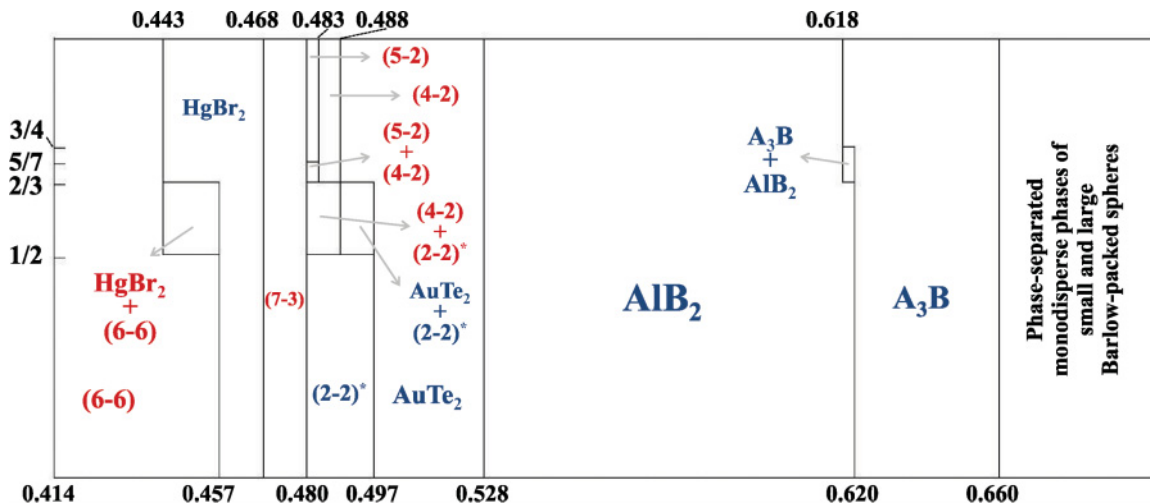


FIG. 14. (Color online) Phase diagram in (α, ϕ) for $\sqrt{2} \leq \alpha \leq 1$ of the densest-known binary sphere packings in \mathbb{R}^3 considering periodic packings with minimal bases of 12 or fewer spheres. This image is an enlargement of the right hand side of Fig. 5.

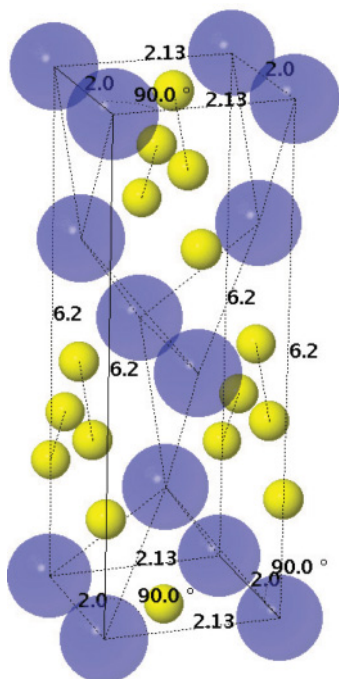


FIG. 15. (Color online) Putative densest packing ($\phi = 0.759$) at radius ratio $\alpha = 0.4597$ of four small and two large spheres in a periodic fundamental cell. The HgBr_2 alloy belongs to the orthorhombic lattice system.

alloy described in Ref. [39], which has four small and four large spheres in its minimal basis. Within the error, we were unable to determine whether doubling the minimal basis from four to eight spheres, just as increasing the minimal basis from four small and four large to six small and six large for the (6-6) alloy, results in an increased packing fraction. We suggest that it might result in an increase of less than 10^{-4} over the approximate range $0.480 \leq \alpha \leq 0.497$ that the alloy

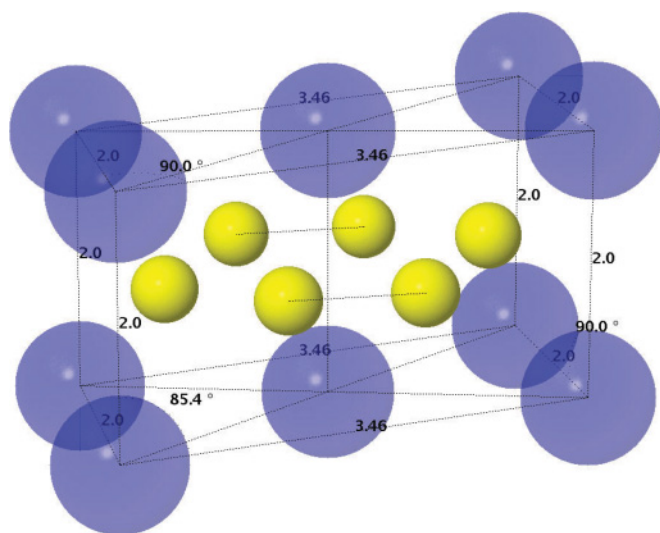


FIG. 16. (Color online) Putative densest packing ($\phi = 0.758$) at radius ratio $\alpha = 0.4995$ of two small spheres and one large sphere in a periodic fundamental cell. The fundamental cell of this AuTe_2 alloy belongs to the monoclinic lattice system.

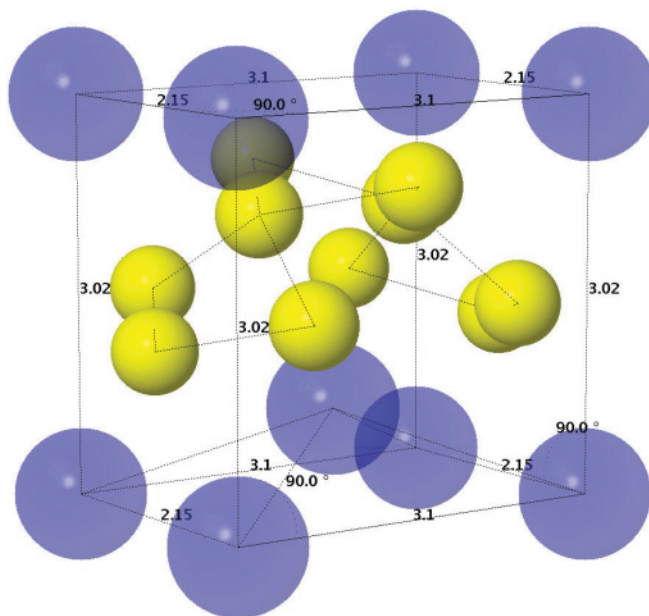


FIG. 17. (Color online) Putative densest packing ($\phi = 0.746$) at radius ratio $\alpha = 0.643$ of six small and two large spheres in a periodic fundamental cell. The A_3B alloy belongs to the orthorhombic lattice system.

appears in the densest packings, though we would need to run simulations at higher accuracy in order to confirm or reject this hypothesis. Figure 18 depicts the fundamental cell of the (2-2)* packing, which belongs to the monoclinic lattice system, at $\alpha = 0.4881$.

The “Structure 1” alloy described in Ref. [39] has a minimal basis of four small and four large spheres. However, our simulations show that increasing the minimal basis to six

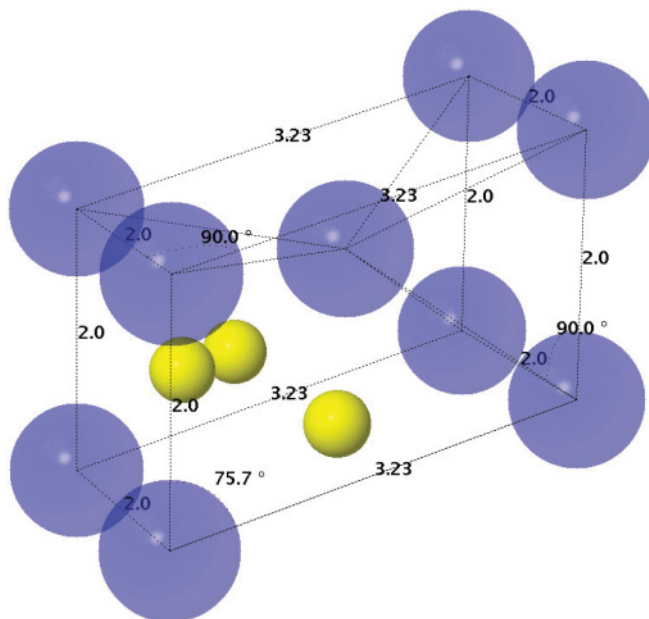


FIG. 18. (Color online) Putative densest packing ($\phi = 0.746$) at radius ratio $\alpha = 0.4881$ of two small and two large spheres in a periodic fundamental cell. The (2-2)* alloy belongs to the monoclinic lattice system.

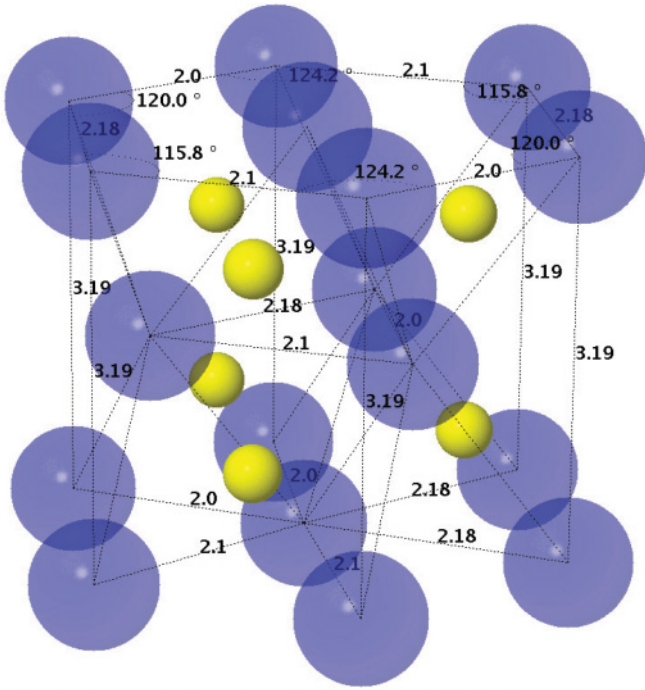


FIG. 19. (Color online) Putative densest packing ($\phi = 0.758$) at radius ratio $\alpha = 0.4483$ of six small and six large spheres in a periodic fundamental cell. The (6-6) alloy belongs to the triclinic lattice system.

small and six large spheres results in the identification of a denser alloy. Specifically, we find (error of less than 10^{-4}) that the (6-6) alloy exhibits the same packing fraction as the Structure 1 alloy over the approximate range $0.414 \leq \alpha < 0.428$ and a denser packing fraction over the approximate range $0.428 \leq \alpha \leq 0.457$. The (6-6) alloy phase, illustrated in Fig. 19, belongs to the triclinic lattice system and is similar to a skewed and stretched version of the NaCl alloy. It is unclear if increasing the minimal basis beyond 12 spheres will result in a slightly denser alloy over the approximate range $0.414 \leq \alpha \leq 0.457$ that the (6-6) alloy appears to be present in the densest packings.

The (7-3) alloy appears in the densest packings over the approximate range $0.468 \leq \alpha \leq 0.480$. Its minimal basis contains seven small and three large spheres, and the alloy belongs to the orthorhombic lattice system. It exhibits a local maximum at $\phi_{\max}(0.474\,568\dots, 7/10) = 0.752\,189\dots$. For $\alpha < 0.474\,568$ where the alloy appears in the densest packings, it is stabilized along the x axis and y axis (the axes parallel to the basis vectors in Fig. 20 shown as having lengths 2.0 and 9.65, respectively) by large-large contacts, and along the z axis it is stabilized by small-large contacts. For $\alpha > 0.474\,568\dots$ where the alloy appears in the densest packings, the y axis is stabilized both by large-large and small-large contacts.

The (5-2) alloy belongs to the monoclinic lattice system and appears in the densest packings only over a very short range of α , approximately $0.480 \leq \alpha \leq 0.483$. This brief appearance is not due to a local maximum in packing fraction in the (5-2) alloy, but rather to the fact that other dense binary alloys, such as the (4-2), HgBr₂, AuTe₂, and (7-3), all happen to exhibit relatively lower packing fractions over this range of α . One

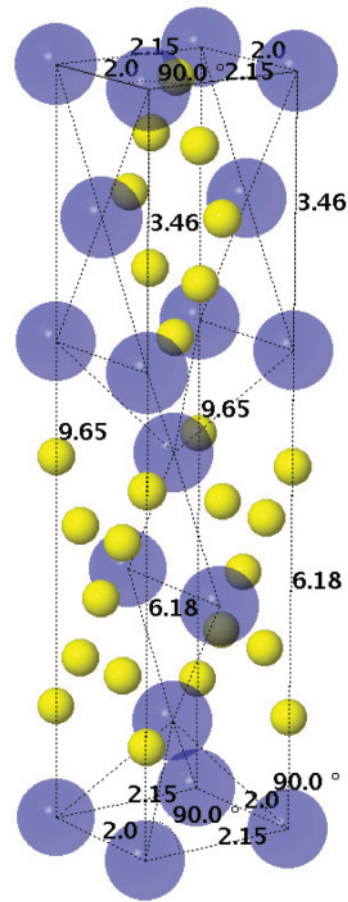


FIG. 20. (Color online) Putative densest packing ($\phi = 0.752$) at radius ratio $\alpha = 0.4682$ of seven small and three large spheres in a periodic fundamental cell. The (7-3) alloy belongs to the orthorhombic lattice system.

notable feature of the (5-2) alloy is a large void space, visible in Fig. 21 just above the four large spheres at the top right of the image.

The (4-2) alloy, illustrated in Fig. 22, is present in the densest packing over the approximate range $0.480 \leq \alpha \leq 0.488$. It has four small and two large spheres in its minimal basis and belongs to the triclinic lattice system. The alloy is very similar in packing fraction to both the AuTe₂ and HgBr₂ alloys over the range of α in which it appears in the densest packings. However, the (4-2) alloy fundamental cell has less symmetry, and the distortion in the cell away from a monoclinic arrangement allows for a slightly increased packing fraction over the range $0.480 \leq \alpha \leq 0.488$ as compared to the AuTe₂ alloy.

D. Another dense packing

The (8-1) alloy is particularly dense over the range $0.244 \leq \alpha \leq 0.253$, but it does not appear in the densest packings. As can be seen in Fig. 23, the (8-1) alloy consists of large spheres arranged in a unit cell belonging to the triclinic lattice system, with small spheres in the primary and secondary interstices. There are six small spheres arranged in a skewed octahedron in each primary interstice, and a small sphere in each secondary interstice, where there are twice as many secondary interstices

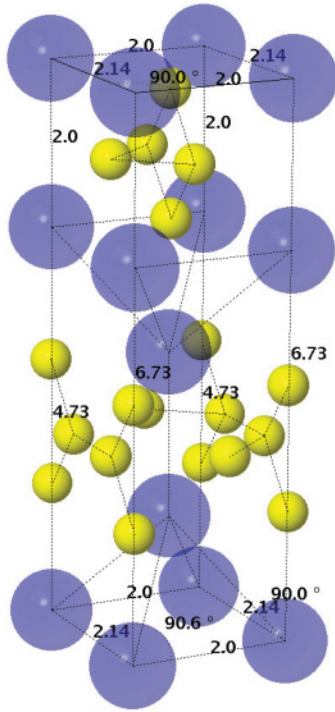


FIG. 21. (Color online) Putative densest packing ($\phi = 0.746$) at radius ratio $\alpha = 0.4824$ of five small and two large spheres in a periodic fundamental cell. The (5-2) alloy belongs to the monoclinic lattice system.

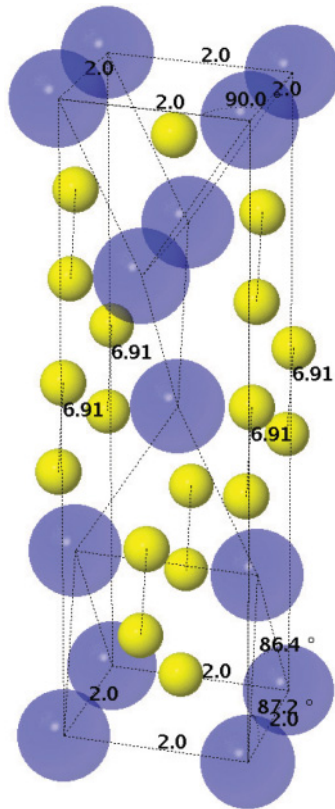


FIG. 22. (Color online) Putative densest packing ($\phi = 0.748$) at radius ratio $\alpha = 0.4853$ of four small and two large spheres in a periodic fundamental cell. The (4-2) alloy belongs to the triclinic lattice system.

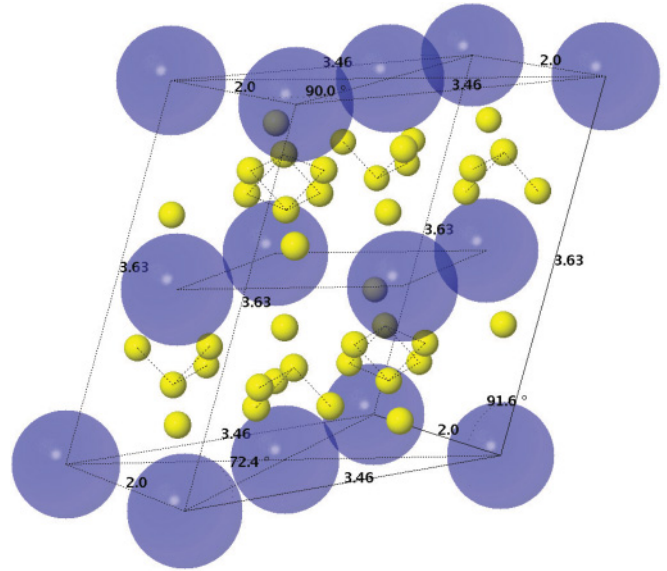


FIG. 23. (Color online) Very dense packing ($\phi = 0.787$) at radius ratio $\alpha = 0.2503$ of eight small and one large spheres in a periodic fundamental cell. This (8-1) alloy did not appear in the densest packings in our simulations; though it is denser over the approximate range $0.244 < \alpha < 0.253$ at $x = 8/9$ than the combination of two phase-separated phases where one is any other known alloy and the other is a monodisperse phase, the combination of two phase-separated alloy phases [the (10-1) and XY_4 phases] is denser. The (8-1) alloy belongs to the triclinic lattice system.

as primary interstices. Interestingly, at $x = 8/9$, the (8-1) alloy is denser than any phase-separated combination of a different alloy phase and a monodisperse phase. Nevertheless, a phase-separated combination of the (10-1) and XY_4 alloy phases permits a denser packing at $x = 8/9$ than a single (8-1) phase.

VI. CONCLUSIONS

We have surveyed the α - x plane at high resolution in both α and x in order to find the densest binary sphere packings in \mathbb{R}^d for minimal bases of up to 12 spheres. Employing an implementation of the TJ algorithm, we have identified all of the previously known alloys present in the densest packings and found many new alloys as well. We have described and presented the structure and symmetries of these densest alloys, and we have classified them by the composition of their minimal bases and lattice system characterization of their unit cells. Taken together, these results demonstrate that there is a broad diversity of alloys present in the densest packings, including alloys with large minimal bases and uncommon small to large sphere number ratios, *e.g.*, the (6-6), (7-3), and (5-2) alloys.

We have also discussed the densest binary packings in \mathbb{R}^3 , which are composed of phase-separated densest Barlow and alloy phases. We have proved that for any packing consisting of η different types of objects in \mathbb{R}^d , there is a densest packing that consists of no more than η different phases. Additionally, we have discussed the properties of the function $\phi_{\max}(\alpha, x)$ and described its features in the limit as $(\alpha, x) \rightarrow (0, 1)$.

One implication of our findings is that that entropic (free-volume maximizing) particle interactions contribute to the structural diversity of mechanically stable and ground-state structures of atomic, molecular, and granular solids. Additionally, the structures we have identified can be useful as known points of departure when investigating experimentally the properties of binary solids composed of particles that exhibit steep isotropic pair repulsion, including those in dense atomic and molecular phases at high temperatures and pressures. In particular, some of the unique structures that we have identified could correspond to currently unidentified stable atomic and molecular states of matter. We note though that these structures would be most relevant to binary phases, perhaps at high temperatures and pressures, where the two particle types exhibit roughly additive pair repulsion.

Though we have limited ourselves in this work to minimal bases of 12 or fewer spheres, the discovery of the (7-3), (6-6), and (5-2) alloys suggests that periodic structures with minimal bases larger than 12, further directionally periodic, quasicrystalline, and disordered structures might be present among the densest packings. This may also include a densest alloy, composed of a minimal basis of greater than 12 spheres, for $\alpha > \alpha^*$.

It is possible that the densest packings we have identified have a relation to the structures of glassy binary sphere solids and/or to those of binary sphere liquids near the freezing point. For example, recent work [55] demonstrates that a binary metallic glass, $\text{Ce}_{75}\text{Al}_{25}$ ($x = 1/4$, with the atomic volume of Ce about twice that of Al at ambient pressure), exhibiting long-range structural order can be created by a melt-spinning process. Further investigation suggests that the long-range fcc order is derived from the binary material's densely packed configuration during spinning. It is possible that other binary glasses could exhibit similar long-range order related to the densest packings of binary spheres at specified (α, x) .

In future work, we will employ the TJ algorithm to study maximally random jammed (MRJ) packings of binary spheres at specified (α, x) . This is a complicated problem, in part due to the difficulty in defining a MRJ state for binary packings. Nevertheless, a thorough investigation may reveal similarities between the MRJ packings and the densest binary packings at the same radius ratios α and small sphere relative concentrations x .

ACKNOWLEDGMENTS

This work was supported by the MRSEC Program of the National Science Foundation under Award No. DMR-0820341. The simulations of dense binary sphere packings using the TJ algorithm were performed primarily on computational resources supported by the Princeton Institute for Computational Science and Engineering (PICSciE) and the Office of Information Technology's High Performance Computing Center and Visualization Laboratory at Princeton University.

APPENDIX A: IMPLEMENTATION OF THE ALGORITHM

The implementation of the TJ algorithm for binary spheres requires a multistep process. This multistep process is run

many times with many different initial configurations of spheres, in particular over initial configurations where the positions of large and small spheres are interchanged within a periodic unit cell.

In the first step of the process, an initial configuration of nonoverlapping small and large spheres is generated. This is accomplished through a random sequential addition [8] process of adding large spheres to a randomly generated unit cell, then choosing which spheres will be designated small and which will be large. The cell is randomly generated in \mathbb{R}^3 using five random variables which represent the angles between the three lattice vectors and the relative lengths of the second and third lattice vectors to the first, which is normalized. The angles and lattice vector lengths are required to fall within certain bounds, and the total volume of the cell is bounded from below. These bounds are useful algorithmically in preventing overlap between the spheres in the unit cell and their images in nonadjacent unit cells.

The next step is to solve the linear programming problem (5) assuming that $\mathcal{R} = 0$, where we recall that \mathcal{R} represents the higher order terms in the linear expansion of the packing problem and its constraints. After solving the problem (5), it is necessary to check if any overlap is present between spheres in the unit cell or between the spheres in the unit cell and their images in surrounding cells. This step is necessary because \mathcal{R} is sometimes negative, which can result in a solution to the problem (5) with overlap between spheres. The higher order terms \mathcal{R} can be written,

$$\mathcal{R} = 3\Delta\mathbf{r}_{ij} \cdot \mathbf{e}^2 \cdot \Delta\mathbf{r}_{ij} + 2|\mathbf{e} \cdot \mathbf{r}_{ij} + \Delta\mathbf{r}_{ij}|^2 - |\mathbf{e} \cdot (\mathbf{r}_{ij} - \Delta\mathbf{r}_{ij})|^2 - |\Delta\mathbf{r}_{ij} - \mathbf{e} \cdot \Delta\mathbf{r}_{ij}|^2. \quad (\text{A1})$$

The first two terms in Eq. (A1) are positive semidefinite and the last two negative semidefinite. When the last two terms are greater in absolute value than the first two, this indicates that overlap between spheres can exist in a correctly solved linearized programming problem.

If overlap is present between any two spheres, the lattice vectors $\{\lambda_i\}$ are resized by a constant such that all previously overlapping spheres are now out of contact by at least some small $\delta > 0$. All spheres in the packing are subsequently displaced in random directions by small random distances such that all distances are less than or equal to δ . This step is necessary so that the algorithm does not become stuck in a loop. Additionally, the randomness introduced by this step aids in finding densest packings. If no overlap is present, then no resize of the lattice vectors is necessary. In either case, the algorithm repeats until there is no solution to the problem (5) that reduces packing fraction, *i.e.*, the packing is strictly jammed.

APPENDIX B: PROOF OF THEOREM 1

To prove Theorem 1, we will utilize the fundamental theorem of linear programming, which states that there is always a globally optimal solution to a linear programming problem (that has at least one solution) located at (at least) one of the vertices of the convex polytope that is the problem's feasible region. In this case, the objective function of the linear programming problem is the denominator of Eq. (6),

and the feasible region is defined by the constraints on the variables $x_i^{F_i}$ that result from conservation of particle numbers. We first outline these constraints then apply the fundamental theorem of linear programming to prove that for a packing of η different sphere sizes in \mathbb{R}^d there is at least one densest packing composed of no more than η phase-separated phases.

As the $X^{(j)}$ are relative fractions, $\sum_{j=1}^{\eta} X^{(j)} = 1$ and $X^{(j)} \geq 0$ for all j due to conservation of particle numbers. For the same reason, summing up all the relative fractions $x_i^{F_i}$ of spheres of type j in each alloy type i , we have

$$\sum_{i=1}^{\beta} \frac{S_i^j}{S_i^{F_i}} x_i^{F_i} = X^{(j)}, \quad (\text{B1})$$

where we note that each term in the sum on the left hand side of Eqs. (B1) is equal to x_i^j . It follows from Eqs. (B1) and the non-negativity of the $x_i^{F_i}$ that

$$\frac{S_i^j}{S_i^{F_i}} x_i^{F_i} \leq X^{(j)}, \quad (\text{B2})$$

or for each phase i and sphere type j , the relative fraction x_i^j of spheres of type j in phase i is less than or equal to the total relative fraction of spheres $X^{(j)}$ of type j .

For each variable $x_i^{F_i}$, there is one or more indices j with nonzero S_i^j that yields the most restrictive constraint on $x_i^{F_i}$ from Eqs. (B2), *i.e.*, one that yields the minimum value of $X^{(j)}/S_i^j$ from among all j . To be consistent with previous index nomenclature, we term this first such index J_i . Employing this form, the Eqs. (B2) reduce to β inequalities that together with the non-negativity of the $x_i^{F_i}$ produce the β bounds,

$$0 \leq x_i^{F_i} \leq \frac{S_i^{J_i}}{S_i^{F_i}} X^{(J_i)}, \quad (\text{B3})$$

which describe a hyper-rectangular prism in β -dimensional Euclidean space in the variables $x_i^{F_i}$.

The η equations (B1) describe η hyperplanes in β -dimensional Euclidean space. The convex polytope that forms the feasible region consists of their intersection with each other and the hyper-rectangular prism described by inequalities (B3). We can thus formulate a linear programming problem corresponding to the maximum of Eq. (6) as

$$\min \sum_{i=1}^{\beta} \frac{C_i}{S_i^{F_i}} x_i^{F_i}, \quad (\text{B4})$$

subject to the equality constraints (B1) and the inequality constraints (B3). This allows us to prove Theorem 1, as follows.

Proof. Due to the monodisperse alloys, the hyperplanes defined by Eqs. (B1) have at least one point of mutual intersection. Terming the relative fractions of the monodisperse alloys $x_1^1, \dots, x_\eta^\eta$, this point is $\{x_1^1, \dots, x_\eta^\eta\} = \{X^{(1)}, \dots, X^{(\eta)}\}$ and $\{x_i^{F_i} = 0; i > \eta\}$, namely, the packing where all phases are monodisperse. As this point is contained within the feasible region, we can apply the fundamental theorem of linear programming to state that there is a globally optimal solution to the problem (B4) located at (at least) one of the vertices of the convex polytope formed by the intersection of the η

hyperplanes described by Eqs. (B1) and the hyper-rectangular prism described by inequalities (B3).

To prove that there is a globally optimal solution that consists of no more than η phase-separated phases, we show that there can be no more than η positive values of $x_i^{F_i}$ at any of the vertices of the feasible region. To this end, we first describe the vertices of the feasible region where the η hyperplanes intersect the hyper-rectangular prism only at the lower bounds of inequalities (B3). Immediately following, we describe the vertices when the η hyperplanes intersect at one or more of the upper bounds of inequalities (B3).

The vertices where the η hyperplanes intersect only at the lower bounds of the hyper-rectangular prism consist of all combinations of no more than η positive $x_i^{F_i}$ and no fewer than $\beta - \eta$ zero values of $x_i^{F_i}$ such that Eqs. (B1) are satisfied. There can be no more than η nonzero $x_i^{F_i}$ at a vertex because the vertices must occur where at least β equality constraints are satisfied, *i.e.*, where $x_i^{F_i} = 0$ on at least $\beta - \eta$ of the half planes described by the inequalities (B3), and at the intersection of the η hyperplanes described by Eqs. (B1). There can be fewer than η positive $x_i^{F_i}$, in particular if the intersection of the η d -dimensional hyperplanes describes a hyperplane embedded in β dimensions that is more than $(\beta - \eta)$ -dimensional or if one of the η hyperplanes happens to intersect with the half plane described by one of the lower bounds of the inequalities (B3) at a given vertex where all nonzero $x_i^{F_i}$ are positive.

If the intersection of the η hyperplanes simultaneously intersects t faces of the hyper-rectangular prism at the upper bounds of inequalities (B3), then for a set of t indices $\{q\}_t$, $x_q^{F_q} = (S_q^{F_q}/S_q^{J_q})X^{(J_q)}$. At all points contained within this intersection, all spheres of types J_q are present only in their respective phases q . This means that for all other $x_i^{F_i}$ where phase i includes any spheres of types J_q , $x_i^{F_i} = 0$. Excluding these phases and the phases $\{q\}_t$, the problem is reduced to the remaining β_t variables with indices $\{i\}_t$ in β_t dimensions and where there are $\eta - t$ constraints of the form

$$\sum_{\{i\}_t} \frac{S_i^j}{S_i^{F_i}} x_i^{F_i} = X^{(j)} - \sum_{\{q\}_t} \frac{S_q^j}{S_q^{F_q}} x_q^{F_q}. \quad (\text{B5})$$

In Eqs. (B5), the index j is for all $j = 1, \dots, \eta$ excluding the $j = \{J_q\}$, the sum on the left hand side runs over the β_t indices included in the set $\{i\}_t$, and the sum on the right hand side runs over the t indices included in the set $\{q\}_t$.

In this reduced case, the Eqs. (B5) imply new upper bounds on the β_t remaining $x_i^{F_i}$ which describe a new hyper-rectangular prism in β_t variables. However, the lower bounds on the β_t variables $x_i^{F_i}$ over the indices $\{i\}_t$ are the same; consequently, the vertices of the feasible region where the $\eta - t$ hyperplanes described by Eqs. (B5) intersect the reduced hyper-rectangular prism only at its lower bounds include no more than $\eta - t$ positive $x_i^{F_i}$ and no fewer than $\beta_t - \eta + t$ zero values of the remaining $x_i^{F_i}$. Coupled with the $\beta - \beta_t - t$ zero values of $x_i^{F_i}$ that include spheres of types J_q and the t values $x_q^{F_q} = (S_q^{F_q}/S_q^{J_q})X^{(J_q)}$, this gives no more than η positive $x_i^{F_i}$ and no fewer than $\beta - \eta$ zero values of $x_i^{F_i}$.

TABLE I. Selected densest binary alloy packing fractions.

α	(11-1)	(10-1)	(6-1) ₁₀	(6-1) _{4,6,8}	α	(6-6)	(7-3)	(5-2)	(4-2)	(2-2)*
0.217	0.823				0.414	0.793				
0.220	0.818				0.417	0.789				
...					0.420	0.786				
0.225		0.825			0.423	0.783				
0.228		0.822			0.426	0.779				
0.230		0.820			0.428	0.776				
0.233		0.818			0.431	0.773				
...					0.434	0.771				
0.245		0.804			0.437	0.768				
0.247		0.800			0.440	0.765				
0.250		0.797			0.443	0.763				
0.253		0.794			0.445	0.760				
0.256		0.791			0.448	0.758				
0.258		0.789			0.451	0.756				
0.261		0.787			0.454	0.754				
0.264		0.785	0.781		0.457	0.751				
0.267		0.783	0.782		0.460					
0.270		0.781	0.784		0.463					
0.273			0.785		0.465					
0.275			0.787		0.468		0.752			
0.278			0.789		0.471		0.752			
0.281			0.792		0.474		0.752			
0.284			0.794		0.477		0.750			
0.287			0.797		0.480		0.748	0.746	0.744	0.744
0.289			0.800		0.483			0.746	0.746	0.744
0.292			0.801		0.485				0.748	0.745
0.295				0.800	0.488				0.750	0.746
0.298				0.799	0.491					0.747
0.301				0.798	0.494					0.748
0.304				0.797	0.497					0.749
0.307				0.797						
0.309				0.796						
0.312				0.795						
0.315				0.794						
0.318				0.793						
0.321				0.792						
0.324				0.788						
0.326				0.786						
0.329				0.783						
0.332				0.780						
0.335				0.778						
0.338				0.775						
0.341				0.773						
0.343				0.771						
0.346				0.769						
0.349				0.768						
0.352				0.766						

The value t cannot exceed η because at $t = \eta$, $\beta_t = 0$, as all phases must include at least one type of sphere. It follows that all vertices must include between $t = 0$ and $t = \eta$ intersections at the upper bounds of the hyper-rectangular prism, and so we have proved that there cannot be more than η positive $x_i^{F_i}$ at any vertex. It follows directly, since there is at least one global optimum on a vertex, that there is always at least one densest packing that includes no more than η phase-separated phases. ■

We note that there can also be global minima that include more than η phases. This occurs when there is more than one vertex that is a global optimum such that there are more than η distinct nonzero $x_i^{F_i}$ in total in the optimal vertices. Specifically, when there is more than one vertex that is a global optimum, all convex combinations of these vertices are also global optima. This leads to the conclusion that of β possible phases, there could potentially be β phases present in a densest packing, with β unbounded.

APPENDIX C: PACKING FRACTIONS

The packing fractions in this appendix are for the periodic alloys that comprise the densest packings at given values of α . By comparing the alloys found by the algorithm to densest alloys for which we have explicit representations of the packing fraction, we have discovered that the packing fractions are in general about 1.0×10^{-4} too low, though sometimes as much as 2.5×10^{-4} too low. For this reason, and due to the resolution of our survey in α , we report packing

fractions only to the third decimal place. Additionally, we note that our algorithm, being constructive, always produces packing fractions for real packings, and therefore the fractions presented are all lower bounds on the true maximal fractions. Finally, we note that although the comparisons we have made in the text to explicitly known packing fractions are for the precise values of α that we employed in our survey, the values of α reported in this table have been rounded to the third decimal place.

-
- [1] S. Torquato and F. H. Stillinger, *Rev. Mod. Phys.* **82**, 2633 (2010).
- [2] G. L. Pollack, *Rev. Mod. Phys.* **36**, 748 (1964).
- [3] J. V. Sanders, *Philos. Mag. A* **42**, 705 (1980).
- [4] P. Bartlett, R. H. Ottewill, and P. N. Pusey, *Phys. Rev. Lett.* **68**, 3801 (1992).
- [5] M. J. Vlot, H. E. A. Huitema, A. de Vooy, and J. P. van der Eerden, *J. Chem. Phys.* **107**, 4345 (1997).
- [6] T. F. Middleton, J. Hernandez-Rojas, P. N. Mortenson, and D. J. Wales, *Phys. Rev. B* **64**, 184201 (2001).
- [7] M. Amsler and S. Goedecker, *J. Chem. Phys.* **133**, 224104 (2010).
- [8] S. Torquato, *Random Heterogeneous Materials* (Springer-Verlag, New York, 2002).
- [9] P. M. Chaikin and T. C. Lubensky, *Principles of Condensed Matter Physics* (Cambridge University Press, Cambridge, 1995).
- [10] J. P. Hansen and I. R. McDonald, *Theory of Simple Liquids*, 3rd ed. (Academic Press, Amsterdam, 2006).
- [11] R. Zallen, *The Physics of Amorphous Solids* (Wiley & Sons, New York, 1983).
- [12] A. B. Hopkins, F. H. Stillinger, and S. Torquato, *Phys. Rev. E* **79**, 031123 (2009).
- [13] A. B. Hopkins, F. H. Stillinger, and S. Torquato, *J. Math. Phys.* **51**, 043302 (2010); *Phys. Rev. E* **81**, 041305 (2010); **83**, 011304 (2011).
- [14] A. Donev, F. H. Stillinger, P. M. Chaikin, and S. Torquato, *Phys. Rev. Lett.* **92**, 255506 (2004).
- [15] Y. Jiao, F. H. Stillinger, and S. Torquato, *Phys. Rev. E* **79**, 041309 (2009); R. D. Batten, F. H. Stillinger, and S. Torquato, *ibid.* **81**, 061105 (2010).
- [16] S. Torquato and Y. Jiao, *Nature (London)* **460**, 876 (2009); *Phys. Rev. E* **80**, 041104 (2009); **81**, 041310 (2010).
- [17] E. Chen, *Disc. Comp. Geom.* **40**, 214 (2008); E. Chen, M. Engel, and S. Glotzer, *ibid.* **44**, 253 (2010).
- [18] Y. Kallus, V. Elser, and S. Gravel, *Disc. Comp. Geom.* **44**, 245 (2010).
- [19] J. de Graaf, R. van Roij, and M. Dijkstra, *Phys. Rev. Lett.* **107**, 155501 (2011).
- [20] Y. Jiao and S. Torquato, *Phys. Rev. E* **84**, 041309 (2011); *J. Chem. Phys.* **135**, 151101 (2011).
- [21] F. Ding and N. V. Dokholyan, *Trends Biotechnol.* **23**, 450 (2005); N. V. Dokholyan, *Curr. Opin. Struct. Biol.* **16**, 79 (2006); C. H. Davis, H. Nie, and N. V. Dokholyan, *Phys. Rev. E* **75**, 051921 (2007).
- [22] D. Drasdo and S. Höhme, *Phys. Bio.* **2**, 133 (2005).
- [23] J. L. Gevertz, G. Gillies, and S. Torquato, *Phys. Biol.* **5**, 036010 (2008); J. L. Gevertz and S. Torquato, *PLoS Comp. Biol.* **4**, e1000152 (2008).
- [24] G. M. Knott, T. L. Jackson, and J. Buckmaster, *AIAA J.* **39**, 678 (2001); S. Kochevets, J. Buckmaster, T. L. Jackson, and A. Hegab, *J. Propul. Power* **17**, 883 (2001); F. Maggi, S. Stafford, T. L. Jackson, and J. Buckmaster, *Phys. Rev. E* **77**, 046107 (2008).
- [25] M. Kolonko, S. Raschdorf, and D. Wäsch, *Granular Matter* **12**, 629 (2010).
- [26] W. Hume-Rothery, R. E. Smallman, and C. W. Haworth, *The Structure of Metals and Alloys*, 5th ed. (Metals and Metallurgy Trust, London, 1969).
- [27] M. J. Murray and J. V. Sanders, *Philos. Mag. A* **42**, 721 (1980).
- [28] S. K. Sikka, Y. K. Vohra, and R. Chidambaram, *Prog. Mater. Sci.* **27**, 245 (1982).
- [29] A. R. Denton and N. W. Ashcroft, *Phys. Rev. A* **42**, 7312 (1990).
- [30] M. D. Eldridge, P. A. Madden, and D. Frenkel, *Nature (London)* **365**, 35 (1993); *Mol. Phys.* **79**, 105 (1993); **80**, 987 (1993).
- [31] X. Cottin and P. A. Monson, *J. Chem. Phys.* **99**, 8914 (1993); **102**, 3354 (1995).
- [32] M. Widom and M. Mihalkovic, *J. Mater. Res.* **20**, 237 (2005).
- [33] A. B. Hopkins, Y. Jiao, F. H. Stillinger, and S. Torquato, *Phys. Rev. Lett.* **107**, 125501 (2011).
- [34] S. Torquato and Y. Jiao, *Phys. Rev. E* **82**, 061302 (2010).
- [35] K. Y. Szeto and J. Villain, *Phys. Rev. B* **36**, 4715 (1987).
- [36] P. I. O'Toole and T. S. Hudson, *J. Phys. Chem. C* **115**, 19037 (2011).
- [37] L. Fillion and M. Dijkstra, *Phys. Rev. E* **79**, 046714 (2009).
- [38] C. N. Likos and C. L. Henley, *Philos. Mag. B* **68**, 85 (1993).
- [39] G. W. Marshall and T. S. Hudson, *Contr. Alg. Geo.* **51**, 337 (2010).
- [40] R. Demchyna, S. Leoni, H. Rosner, and U. Schwarz, *Z. Kristallogr.* **221**, 420 (2006).
- [41] C. Cazorla, D. Errandonea, and E. Sola, *Phys. Rev. B* **80**, 064105 (2009).
- [42] V. Degtyareva, *J. Synchrotron Radiat.* **12**, 584 (2005).
- [43] T. C. Hales, *Ann. Math.* **162**, 1065 (2005).
- [44] W. Barlow, *Nature (London)* **29**, 186 (1883).
- [45] T. S. Hudson and P. Harrowell, *J. Phys. Chem. B* **112**, 8139 (2008).
- [46] J. K. Kummerfeld, T. S. Hudson, and P. Harrowell, *J. Phys. Chem. B* **112**, 10773 (2008).

- [47] L. Filion, M. Marechal, B. van Oorschot, D. Pelt, F. Smalenburg, and M. Dijkstra, *Phys. Rev. Lett.* **103**, 188302 (2009).
- [48] L. Bindi, P. J. Steinhardt, N. Yao, and P. J. Lu, *Science* **324**, 1306 (2009).
- [49] D. Levine and P. J. Steinhardt, *Phys. Rev. B* **34**, 596 (1986).
- [50] L. F. Toth, *Regular Figures* (Macmillan, New York, 1964).
- [51] P. W. Leung, C. L. Henley, and G. V. Chester, *Phys. Rev. B* **39**, 446 (1989).
- [52] M. Widom, *Phys. Rev. Lett.* **70**, 2094 (1993).
- [53] S. Torquato, T. M. Truskett, and P. G. Debenedetti, *Phys. Rev. Lett.* **84**, 2064 (2000); S. Torquato and F. H. Stillinger, *J. Phys. Chem B* **105**, 11849 (2001).
- [54] L. Filion, M. Hermes, R. Ni, E. C. M. Vermolen, A. Kuijk, C. G. Christova, J. C. P. Stiefelhagen, T. Vissers, A. van Blaaderen, and M. Dijkstra, *Phys. Rev. Lett.* **107**, 168302 (2011).
- [55] Q. Zeng, H. Sheng, Y. Ding, L. Wang, W. Yang, J.-Z. Jiang, W. L. Mao, and H.-K. Mao, *Science* **332**, 1404 (2011).